

TURTLE: A C LIBRARY FOR AN OPTIMISTIC STEPPING THROUGH A TOPOGRAPHY

A PREPRINT, DECEMBER 15, 2024

Valentin Niess^{a*}, Anne Barnoud^b, Cristina Cârloganu^a, and Olivier Martineau-Huynh^c

^aUniversité Clermont Auvergne, CNRS/IN2P3, LPC, F-63000 Clermont-Ferrand, France

^bUniversité Clermont Auvergne, CNRS, IRD, OPGC, Laboratoire Magmas et Volcans, F-63000
Clermont-Ferrand, France

^cSorbonne Université, Université Paris Diderot, Sorbonne Paris Cité, CNRS, Laboratoire de
Physique Nucléaire et de Hautes Energies (LPNHE), 4 place Jussieu, F-75252, Paris Cedex 5,
France

ABSTRACT

TURTLE is a C library providing utilities allowing to navigate through a topography described by a Digital Elevation Model (DEM). The library has been primarily designed for the Monte-Carlo transport of particles scattering over medium to long ranges, e.g. atmospheric muons. But, it can also efficiently handle ray tracing problems with very large DEMs (10^9 nodes or more), e.g. for neutrino simulations. The TURTLE library was built on an *optimistic* ray tracing algorithm, detailed in the present paper. This algorithm allows to traverse a topography in constant time, i.e. independently of the number of grid nodes, and with no added memory. Detailed performance studies are provided by comparison to other ray tracing algorithms and as an application to muon transport in a Monte-Carlo simulation.

Keywords : Topography · Ray tracing · Monte-Carlo · Transport

1. Introduction

High Energy Physics Monte-Carlo (HEPMC) simulations are a key element of many (astro)particle physics experiments. Some problems require to transport elementary particles over tens to hundreds of km, in a complex outdoor environment. This is for example the case for muography measurements or for experiments searching extraterrestrial neutrinos. Muography is a particularly complex case since particles might scatter a lot, e.g. by grazing the ground and interacting with surface structures. Accurate Monte-Carlo computations then require a detailed but efficient description of the topography over large distances.

Topography data are provided by Digital Elevation Model(s) (DEM), one or a combination of DEMs with different resolutions. A DEM can represent various information, e.g. the surface

*niess@in2p3.fr

above ground structures and the canopy, the ground level, the sea level (geoid undulations) w.r.t. a reference ellipsoid. The elevation data are stored over a regular grid in geodetic coordinates (latitude, longitude) or projected coordinates, e.g. Universal Transverse Mercator (UTM). Note that unordered meshes exist as well, but they are not considered in the following. Elevation values are typically encoded over 2 bytes (`int16_t`) per grid node. Large scale data sets comprise 10^8 to 10^9 nodes resulting in a hundreds of MB to a few GB memory footprint. Due to the Earth curvature, when transformed to the Cartesian laboratory frame of the simulation, the grid nodes are no longer equally spaced. Planarity is lost as well over large distances. For example two nodes at the same elevation above sea level, but distant by 10 km, are actually vertically separated by about 8 m in the laboratory frame.

In HEPMC simulations, a geometry is defined as a collection of closed volumes, bounded by surfaces, and filled with various materials. The transport through the geometry is simulated by discrete steps following straight lines. Each Monte-Carlo step involves a ray tracing problem. Ray tracing is a generic geometry problem. For example, it is also encountered when rendering high quality 3D scenes in computer graphics, since it allows to account for physical effects like light reflection and refraction. However, in a HEPMC the ray length can be drastically limited by the physics, as stochastic interactions occur with the matter of volumes. This leads to changes in the particle direction of propagation, requiring specific ray tracing optimisations. The pseudocode [1](#) describes a simple transport algorithm in order to guide the following discussion.

A HEPMC transport engine navigates through the geometry using the pseudocode functions: `volume_at` and `distance_to`. The former function returns a reference to the volume at a given position, \vec{r} . The later one provides the distance to the closest boundary surface, along a direction, \vec{u} , if specified. When volumes are explicitly connected, the next volume can also be returned. Some Monte-Carlo engines, like MCNP [\[1–3\]](#), enforce this when defining the geometry. Otherwise the next volume must be found using the `volume_at` function. Note that an underestimate for the distance to the next volume can be returned instead of the exact one. The pseudocode expects a reference to the current volume to be returned in this case. Underestimates, independent of the particle direction, are fast to compute for usual geometric shapes: cube, sphere, ... In the case where the Monte-Carlo navigation is limited by the physics, $\lambda < s$ for most steps, then using underestimates speeds up the navigation. This strategy is used by the Geant4 [\[4–6\]](#) generic HEPMC package. Geant4 is a popular Monte-Carlo engine for particle physics. It was originally designed for modelling the interactions of high energy particles within particle physics detectors. The Geant4 engine is flexible though, and there have been many other applications, e.g. in medical physics or for space radiation studies. We illustrate the following discussion with several concrete references to Geant4.

In the following, for the sake of clarity, we consider a simple geometry with only two volumes: the atmosphere and the Earth, separated by a ground surface. The ground surface is usually approximated as a collection of plane facets joining the DEM nodes. Tessellating a regular grid with triangles requires 2 triangles per node. In Geant4 such a tessellation is represented by a `G4TessellatedSolid` object. Building an efficient 3D model for a non parametric volume containing billions of facets is rather involved. The memory overhead should be carefully controlled. For example, adding a single `float32_t` per node already triples the memory usage. At the same

Pseudocode 1: Simple transport algorithm for a HEPMC

```

Input:  $\vec{r}, \vec{u}$  % The particle position and direction

begin
  % Get the initial volume
  volume = volume_at( $\vec{r}$ )

  % Iterate until something happens
  while ...
    % Get the step limit from the physics
     $\lambda \leftarrow$  physics_distance(volume,  $\vec{r}$ , ...)

    % Get the distance to the next volume, or an underestimate
    s, next  $\leftarrow$  distance_to(volume,  $\vec{r}$ ,  $\vec{u}$ ,  $\lambda$ )

    if  $s \geq \lambda$  then
      % Limit the step according to the physics
       $s \leftarrow \lambda$ 
    else
      % Update the volume
      if next then
        volume  $\leftarrow$  next
      else
        volume  $\leftarrow$  volume_at( $\vec{r}$ )
      end
    end

    % Update the particle properties
     $\vec{r} \leftarrow \vec{r} + s\vec{u}$ 
    ...
  end
end

```

time, the geometry must be smartly organised in order to hasten intersection searches. Organizing the geometry must be fast enough as well, i.e. not longer than running a simulation.

A generic optimisation method is to sort geometric shapes (volumes, faces, ...) using a Bounding Volume Hierarchy (BVH). The shapes are organised in a tree structure, according to their bounding boxes. The tree is sorted in order to hasten subsequent geometry operations, e.g. computing the intersection of the shapes with a line or with a plane. BVH trees are used in 3D modelling for ray tracing or collision detection. A popular structure is the Axis Aligned minimum Bounding Box (AABB) tree. It is simple to implement while being efficient. Building the tree using a top down approach is rather fast in addition. A similar approach has long been used in Geant4. It is known as `SmartVoxels`, see e.g. Cosmo [7]. Since Geant4.9.6 (February 2013), this optimisation also propagates down to the individual facets of a `G4TessellatedSolid`. Before, a single bounding box was used for the whole tessellated solid.

Optimising the Geant4 navigation for volumes bounded by a tessellated surface, or by 3D meshes, is a problem that has been previously investigated, e.g. for medical physics applications. In partic-

ular, it was pointed out by Poole et al. [8] that for physics limited navigation, a polyhedral meshing of a volume interior can be more efficient than tessellating its bounding surface. Dividing the interior of a volume in virtual sub-volumes naturally provides fast underestimates of the distance to the next boundary. Unfortunately, this study was done before Geant4.9.6 release, such that no BVH optimisation was applied to the tessellated surfaces used for the comparison. BVH (`SmartVoxels`) were however used for the polyhedral mesh, which makes the comparison unfair. Nevertheless, the point raised by Poole et al. is relevant. The performances of a geometry optimisation depend on the physics case, e.g. on the nature of the propagating particle, on its energy, . . .

For regular DEM grids, the memory overhead due to the geometry modelling can be kept down to zero. The geometry can be fully computed on the fly from the initial elevation data. In Geant4, for a polyhedral mesh, this could be done with a `G4VPVParameterisation`. For a tessellated surface, a dedicated `G4VFacet` should be implemented, using a face parametrisation as well. The current implementation (Geant4.10.5), using static `G4TriangularFacet`, requires 384 bytes per node. This makes this structure impractical for large scale simulations.

In the case of a regular polyhedral mesh, there exists a natural alternative to BVH trees, with zero memory cost: the nodes connectivity. In this case, the exit face from a polyhedron determines the next volume on the grid. This allows to traverse the full grid in $\mathcal{O}(\sqrt{n})$ operations, n being the number of nodes. In comparison, a BVH tree could in principle perform the same in $\mathcal{O}(\log(n))$ operations. Nevertheless, the former algorithm costs no extra memory when the grid is regular. In addition, it could be more efficient when the navigation is limited by the physics. This strategy is used in Geant4 with the `G4VNestedParameterisation`. However this entity paves the space with identical parallelepipeds. Therefore it can not be used for a DEM in a straightforward way.

To conclude on this topic, let us point out that approximating a topographic surface with flat triangular faces between the nodes is a poor man solution. Instead, higher degree interpolations could be used. With additional developments, one might replace the flat faces by smooth surfaces between the nodes, e.g. splines or NURBS. However, we propose a much simpler and straightforward solution to overcome all the previously discussed issues, namely memory usage, stepping efficiency and accuracy. This solution is called *optimistic* algorithm in the following. It implies computing an approximate distance to the next volume, rather than an exact one. The compromise of using an approximate stepping is motivated by the fact that elevation values provided by a DEM are actually space averages around the node coordinates. The typical accuracies of such models is of the order of 10 cm (see e.g. Mukherjee et al. [9]). This *optimistic* algorithm is discussed in section 2. It is the baseline of the TURTLE library, described in section 3.

2. The *optimistic* stepping algorithm

An approximate solution to the ray tracing problem is to proceed by trials and errors. When navigating through the DEM data, a tentative (*optimistic*) stepping distance is proposed for the topography, at each Monte-Carlo step. If the step leads to a ground crossing, the boundary is found with a binary search. The stepping distance is reduced iteratively, in order to converge to the boundary. Otherwise, the step is accepted. Consequently this method has a non null failure rate. If the initial step length, s_0 , is too long, one might overrun some details of the topography, of size

smaller than s_0 . Setting a small enough constant initial value, e.g. $s_0 = 1$ cm mitigates the risk but is very inefficient.

Yet, in the case of a ground surface described by a DEM, a simple yet efficient guess for the initial stepping distance, s_0 , is:

$$s_0 = \max(\alpha|h_0 - g_0|, s_{\min}) \quad (1)$$

where h_0 is the current altitude of the particle and g_0 the corresponding ground level, i.e. $|h_0 - g_0|$ is the height w.r.t. the ground. Using this initial guess instead of a constant one, can provide impressive speed-up, by several orders of magnitude as shown in section 5, without any loss of accuracy.

The parameters $\alpha \leq 1$ and s_{\min} , in eq. (1), are two tuning factors. Let us call them slope factor and resolution factor in the following. The driving idea is that as long as slopes are not too steep, the height w.r.t the ground is a safe estimate of the closest distance to the ground. Reducing the slope factor allows to handle steeper slopes. Setting α below 1 is not efficient for strictly vertical trajectories. Yet, the muography or neutrino transport simulations that we are concerned with deal with close to the horizontal trajectories. The resolution factor plays the role of a safeguard against numerical errors, e.g. close to a boundary. While the boundary is approached with an accurate binary search, it is departed from using a constant step size, given by the resolution factor.

Below are pseudocode implementations of the `volume_at` and `distance_to` functions, using the *optimistic* method and eq. (1) as initial guess for the step length. A key component of the method is the `get_geodetic` function. Given a particle position in the laboratory frame, this function computes its altitude and the corresponding ground level, w.r.t. a same reference, e.g. the sea level. This latter data is efficiently extracted from the DEMs, on the fly, i.e. without building a complete model of the ground surface. This is the main purpose of the TURTLE library. Following, a Monte-Carlo transport engine navigates quickly and simply through the topography, using the *optimistic* approach.

Note that it would be enough to return the signed distance to the ground, $h - g$, from the `get_geodetic` function. However, providing both the particle and ground altitude allows to extend the algorithm by adding extra topography surfaces. For example, one can add a sea volume for $g < h \leq 0$, with altitudes measured w.r.t. the sea level. A sky box can be added as well by checking if $h > h_{\max}$, or an inner structure for the Earth, e.g. following the Preliminary Reference Earth Model (PREM) of Dziewonski and Anderson [10]. When multiple topography surfaces are used, the algorithm discussed in this paper must be slightly modified. An initial guess, s_0 , must be computed for both the surface above and below the current position, using eq. (1). Then the smallest value is used for the tentative step.

Pseudocode 2: Example of `volume_at` function for an *optimistic* stepping through topography data

`Input: \vec{r} % The particle position`

```
Function volume_at( $\vec{r}$ )
     $h, g \leftarrow \text{get\_geodetic}(\vec{r})$ 
    if  $h > g$  then
        return above
```

```

else
    return below
end
end

```

Pseudocode 3: Example of `distance_to` function for an *optimistic* stepping through topography data

```

Input:  $\vec{r}, \vec{u}$       % The particle position and direction
       volume      % A reference to the current volume
        $\lambda$        % A step limit from the physics

Function distance_to(volume,  $\vec{r}$ ,  $\vec{u}$ ,  $\lambda$ )
    % Compute the tentative step length
     $f_0, g_0 \leftarrow \text{get\_geodetic}(\vec{r})$ 
     $s_0 \leftarrow \max(\alpha|h_0 - g_0|, s_{\min})$ 
    if  $s_0 > \lambda$  then  $s_0 \leftarrow \lambda$  end

    % Check the tentative position
    next  $\leftarrow \text{volume\_at}(\vec{r} + s_0\vec{u})$ 

    if next  $\neq$  volume then
        % Locate the topography crossing with a binary search
         $s_1 \leftarrow 0$ 
        while  $s_0 - s_1 > \epsilon$ 
             $s_2 \leftarrow (s_0 + s_1)/2$ 
            volume  $\leftarrow \text{volume\_at}(\vec{r} + s_2\vec{u})$ 
            if volume = next then
                 $s_0 \leftarrow s_2$ 
            else
                 $s_1 \leftarrow s_2$ 
            end
        end
    end

    return  $s_0$ , next
end

```

3. The TURTLE library

TURTLE (Topographic Utilities for tRansporting parTicules over Long rangEs) is a C library providing utilities for stepping through a topography described by a DEM, using the *optimistic* method, described in section 2. The source code of the library is available from GitHub [11] under the GNU LGPL-3.0 license. Version 0.6 is used in this paper. The library was written in C99 and unit-tested on Linux and OSX with a coverage of 90%. An example of Makefile is shipped with the source code allowing to build TURTLE as a shared library, as well as some examples. Note that in addition to the standard C library, TURTLE also requires LibTIFF and libpng in order to read GeoTIFF and PNG files respectively. Though, these functionalities can be disabled with C macros when compiling the library, removing the corresponding dependencies.

TURTLE is not an image processing library neither a Monte-Carlo transport engine. It focuses on few functionalities in order to efficiently track particles over large ranges. These functionalities are exposed to the end user by following an Object Oriented (OO) design, as can be seen by browsing the documentation of the Application Programming Interface (API) [12].

3.1. Maps and projections

The base object of the TURTLE library is an opaque `struct turtle_map` object. It encapsulates a DEM. Those can be loaded from data files with the `turtle_map_load` function. Note that TURTLE can only load a few commonly used data formats for geographic maps: GEOTIFF (e.g. used by ASTER [13]), `*.hgt` (e.g. used by SRTMGL1 [14]) or `*.grd` (e.g. used by EGM96 [15]). Image formats must be 16 bits and grey-scale. New maps can also be created empty and filled using the `turtle_map_create` and `turtle_map_fill` functions. This allows to create custom readers for example. In addition, TURTLE supports dumping and loading maps in PNG, enriched with a dedicated header as a `tEXt` chunk.

The elevation at any position is computed from the DEM with the `turtle_map_elevation` function. A bilinear interpolation is used in order to estimate the elevation. This was chosen over bi-cubic interpolation as a compromise between speed and accuracy. The bilinear interpolation produces a quadratic smoothing in-between the map nodes while being rather fast. However, it generates ridges (discontinuous derivatives) at the borders linking two nodes. With this approach a map keeps in memory no more than the initial elevation data, encoded over 2 bytes per node. The terrain is modelled on the fly when an elevation value is requested. The elevation values at nodes can also be directly inspected using the `turtle_map_node` function. The map meta data can be retrieved with the `turtle_map_meta` function, e.g. the size of the grid.

Local maps, e.g. UTM projections, can have an associated opaque `struct turtle_projection` object. This object allows to convert between the local map coordinates and the geodesic ones, i.e. latitude and longitude. This is done with the `turtle_projection_project` and `turtle_projection_unproject` functions. The `turtle_map_projection` function allows to borrow a pointer to the map projection. `NULL` is returned if the map coordinates are geodesic ones. A projection object can also be directly created (destroyed) using the `turtle_projection_create` (`turtle_projection_destroy`). Note that the projection borrowed from a map should not be explicitly destroyed. It is automatically destroyed when calling `turtle_map_destroy`. The available projections are listed in table 1. The type and parameters of the projection are encoded as a name string at its creation, e.g. `"UTM 31N"` for a UTM projection using zone 31 of the northern hemisphere. A projection can be modified with the `turtle_projection_configure` function. Its name string is provided by the `turtle_projection_name` function. Note that when a map is dumped in PNG format, the projection name string is also written to the file.

3.2. Stacks and clients

World wide models, e.g. ASTER [13] or SRTMGL1 [14] are usually divided in tiles, e.g. of $1 \times 1 \text{ deg}^2$. These models are encapsulated in TURTLE as a `struct turtle_stack` of maps, all maps using geodesic coordinates. When a ground elevation is requested, using `turtle_stack_elevation`, the stack automatically manages loading the right tile into memory.

Projection	Format
Lambert I	"Lambert I"
Lambert II	"Lambert II"
Lambert II extended	"Lambert IIe"
Lambert III	"Lambert III"
Lambert IV	"Lambert IV"
Lambert 93	"Lambert 93"
UTM	"UTM %d%c"
	"UTM %lf%c"

Table 1: List of supported projections in TURTLE v0.6. The format of the name string is indicated following the `printf` semantic.

Tiles are kept in memory until the maximum stack size is reached. In this case the oldest accessed map is removed from memory in order to make room for a newly loaded one. The stack can also be manually cleared with the `turtle_stack_clear` functions. The maximum stack size is specified at the stack creation, using the `turtle_stack_create` functions. Providing a negative or null value disables the automatic deletion of old maps, resulting in all maps being kept in memory, as they are loaded. In some cases it might be more efficient to load all maps in memory right from the start. This is achieved with the `turtle_stack_load` function. At the stack creation one can also provide a couple of `turtle_stack_locker_t` callbacks. These callbacks must provide a lock/unlock mechanism for exclusive data accesses in multithreaded usage, e.g. by managing a semaphore.

Accessing the elevation data directly from a stack object is not thread safe. Instead, for multithreaded usage one must instantiate a `struct turtle_client` of the stack, one per thread. Note that the targeted stack must have lock and unlock callbacks, otherwise an error is generated. The maps usage is monitored by the stack by reference counting. Each client holds a reference to one map at most. When an elevation value is requested, with the `turtle_client_elevation` function, the client first checks if the request belongs to its current map. If not, the client interacts with the stack in order to get access to the right map. The reference to any previous map is dropped as well. Maps with at least one reference cannot be dropped by the stack, even though the stack size is exceeded. Note that switching the client's map requires to lock the stack. However, since we are tracking particles, most of successive elevation accesses are expected to fall within the same map. Therefore, these locks generate no significant retention.

3.3. ECEF coordinates transforms

Elevation maps are provided in geodetic coordinates or using a local projection. Projected coordinates cannot be used directly in a large scale Monte-Carlo where the Earth curvature is no more negligible. A convenient and correct reference frame to use in such Monte-Carlo simulations is the Earth-Centered Earth-Fixed (ECEF) frame. The `turtle_ecef` functions provide coordinate transforms from and to ECEF.

The geodetic to ECEF transform (`turtle_ecef_from_geodetic`) is straightforward, similar to spherical to Cartesian coordinates. The only difference is an ellipticity factor due to the fact that geodetic coordinates are given w.r.t. a reference ellipsoid (WGS84 typically), not a sphere. The reverse transform (`turtle_ecef_to_geodetic`) is less trivial. However it has been extensively studied. We implemented the closed form, yet efficient, provided by Olson [16]. Converting between projected map coordinates and ECEF proceeds through intermediate geodetic coordinates. It requires to project or un-project the local coordinates to or from geodetic ones, such that the `turtle_ecef` functions can be used.

In order to define a direction it is often convenient to use local angular coordinates as for example horizontal ones, i.e. azimuth and elevation. The `turtle_ecef_to_horizontal` and `turtle_ecef_from_horizontal` provide such transforms. Note that the geodetic longitude and latitude must be provided in both cases, in order to define the local East, North, Up (ENU) frame used for the horizontal coordinates.

3.4. The stepper

We now come to the higher level functionalities of TURTLE. The main purpose of the library is to provide tools allowing a Monte-Carlo simulation to step efficiently through a topography, using the *optimistic* approach and ECEF coordinates. The `struct turtle_stepper` object provides an encapsulation of the topography data focused on Monte-Carlo stepping. A `turtle_stepper` is instantiated with the `turtle_stepper_create` function. It starts empty, i.e. without any elevation data. DEMs can be added with the `turtle_stepper_add_map` and `turtle_stepper_add_stack` functions. These functions allow to specify an offset to the native DEM elevation values. A flat topography is specified with the `turtle_stepper_add_flat` function. The last added entry is on the top of the data stack. When an elevation value is requested, the stepper scans its stack down, starting from the top, and it returns the first matching data. This allows to implement different levels of detail, depending on the area of interest. For example, a typical usage would be to have an accurate local map as the top layer, followed by a stack of geodetic maps from a world wide DEM, with a coarser resolution but a larger coverage, and finally a flat Earth as a fallback result for very large distances, when data are missing.

Though not used in this paper, complex geometries can be defined as well by using multiple topography layers. A topography layer can for example specify the depth of the soil, or the level of (sea) water, or the height of the canopy, etc. Adding a topography layer is done with the `turtle_stepper_add_layer` function. Then, multiple data can be added to the new layer, as described previously, i.e. with the `turtle_stepper_add_flat`, `turtle_stepper_add_map` and `turtle_stepper_add_stack` functions. A single DEM can be used in several layers, e.g. with different offset values.

An additional difficulty might arise from the fact that elevation data are usually provided w.r.t. the geoid (sea level), not the ellipsoid. On very large scales this might have an impact since the difference between the two can reach hundred of meters. In this case, when computing ECEF coordinates, one must convert the elevations above the geoid to heights above the ellipsoid. This is done automatically by the stepper by initially providing a map of geoid undulations, e.g. EGM96 [15], with the `turtle_stepper_geoid_add` function.

Once the `turtle_stepper` data is configured, the `turtle_stepper_step` function allows to perform elementary steps through the topography. It has two modes of operation. In both modes, it takes as input an initial position in ECEF.

- (i) When no stepping direction is provided, the function returns the geodetic coordinates at the given ECEF position, the ground level and a tentative stepping distance based on eq. (1).
- (ii) When a stepping direction is provided, the function performs a single step following function `distance_to` described in pseudocode 3. In this case, the function returns the geodetic coordinates at the final position, the corresponding ground level and the actual step length.

Both modes rely on eq. (1). The parameters α and s_{\min} can be modified with the `turtle_stepper_slope_set` and `turtle_stepper_resolution_set` functions. Mode (i) is meant to be integrated in a HEPMC. It provides only a stepping distance, but it actually does not perform any stepping. On the contrary, mode (ii) can be directly iterated in order to step through the topography. However, it is likely to be sub-optimal when integrated within a transport engine, because it does not take into account physical processes nor other volumes, both of which might limit the step length as well.

Computing the ground level at a given position in the laboratory frame requires to convert the ECEF position to the geodetic coordinates used by maps, or to projected ones, e.g. UTM. Doing so can be costly CPU wise, especially when performing a binary search. Therefore the `turtle_stepper` object implements several optimisations. The first one consists in recording any transformed coordinates the first time that a conversion occurs. Similarly, the elevation value of DEMs are recorded after their first access. Then, when the transform or DEM is requested again during the same step, its result is read back from the backup instead of being re-computed. In addition, the stepper also stores a backup of the last outcome of a step, such that it does not need to be computed again if the same position is requested successively. This allows to efficiently chain calls to `turtle_stepper_step`.

Another type of optimisation consists in computing a local linear approximation (LLA) of the transform from the ECEF coordinates to the maps ones, centered on the last computed result. Then, when new positions are requested close enough from the LLA center, the LLA is used instead of the exact computation. The range over which the LLA is used, R_{LLA} , can be configured with the `turtle_stepper_range_set` function. Computing the LLA has a non-negligible CPU cost. It is worth only if one can ensure that the following query actually uses it. Therefore LLAs are computed only if the current step length is smaller than $\frac{R_{LLA}}{3}$, an optimal value selected through trials and errors.

3.5. Error handling

Last, but not least, errors in TURTLE are meant to be managed with a `turtle_error_handler_t` callback. Whenever a library function encounters an error this callback is called. It gets as input an `enum turtle_return` code and a `turtle_function_t`, indicating the type of error that occurred and the faulty function. In addition a brief description of the error is also provided as a string.

The default behaviour is to print the brief error description to `stderr` and to `exit` to the OS. This behaviour can be overridden by providing a custom error handler with the `turtle_error_handler_set` function. Setting the handler to `NULL` disables error handling. Note that in this case, most library functions return a `turtle_return` code in order to indicate their exit status, i.e. `TURTLE_RETURN_SUCCESS` on success, or an error code otherwise.

4. Presentation of the test benches

In the following sections we present the results of various tests and comparisons that have been carried out with the TURTLE library. These tests were run on a dedicated server hosting 64 cores at 2.2 GHz (Intel Xeon E5-4620) with 128 GB of DDR3 memory. Two applications were considered. The first one consists in computing the rock depth along straight lines. Knowing the rock depth along a line of sight is important for muography applications. The muon (μ) flux transmitted through the target indeed depends primarily on the integrated density along the line of sight. Combining the flux measurement with the rock depth thus provides an estimate of the average density of the target. On larger scales, the rock depth close to the horizon is also meaningful in order to estimate the target mass for high energy neutrinos. The first case allows to test the performances of the *optimistic* algorithm as a pure geometry solver. The second application tests the performances of the TURTLE library when integrated in a HEPMC. It consists in computing the spectrum of transmitted atmospheric μ using the PUMAS [17] HEPMC engine.

For both applications we consider 3 view points located in two mountainous areas: Chaîne des Puys in France (fig. 1, left) and Tian Shan in China (fig. 1, right). These areas correspond to real experiments with different topographies and data sets. The first area is taken from muography data acquisition (Ambrosino et al. [18]) targeting the Puy de Dôme volcano, highest summit (1 465 m) of the Chaîne des Puys. The Chaîne des Puys is a north-south oriented chain of ~ 80 volcanoes in the Massif Central in France. It features various volcano shapes: cinder cones, lava domes, craters, We consider two locations where muography detectors have been operated. The first location is south-west of Puy de Dôme: Col de Ceysat (CDC) at 45.764160° N, 2.955385° E, 1 080 m. It is indicated with a black cross on the left plot of fig. 1. The second one is east of Puy de Dôme and slightly lower: TDF building (45.769961° N, 2.980687° E, 927 m), indicated with a red cross.

For the second area we select a single site in the Ulaštai valley. It is a high altitude valley (2 650 m high) in the Tian Shan mountain range. Compared to the Chaîne des Puys this is a rocky area with high and steep summits. The Ulaštai valley is surrounded by 5 000 m high peaks. Ulaštai is hosting the 21 CMA [19] and TREND [20] experiments. The TREND experiment was a seed experiment for the Giant Radio Neutrino Detector (GRAND), see e.g. Alvarez-Muñiz et al. [21]. The location considered is the crossing point of the North-South and East-West arms of the 21 CMA interferometer (42.924211° N, 86.698273° E, 2 534 m). It is indicated with a black dot in the middle of the right plot of fig. 1.

The rock depth seen from the three selected locations was computed using a `turtle_stepper` object. For the Chaîne des Puys area, three topographic data layers are used. The area with the Puy de Dôme is described by a high resolution local DEM with a squared grid of pad size 2.5 m and with 4401×4401 nodes. The local map coordinates are given in Lambert 93 projection. The surrounding area is described by four SRTMGL1 [14] tiles, ranging from latitude 45° N to 47° N

and longitude 2° E to 4° E. Each tile has 3601×3601 nodes and the grid size is approximately ten times larger. The local data set is represented on the left of fig. 1. Outside of this area, a constant ground elevation or zero is assumed. The rock depth through the Puy de Dôme is tracked from the detector locations up to an altitude of 2 000 m, which is slightly above the highest summits of the Massif Central (Puy de Sancy, 1 886 m). 601×301 lines of sight have been scanned with azimuth and elevation values spanning $60 \times 30 \text{ deg}^2$, centered on the Puy de Dôme.

For the Tian Shan area, only two data layers are used, since we have no accurate local topography. The Ulatai valley and its surrounding area is described by 49 SRTMGL1 [14] tiles, ranging from 39° N to 46° N and 83° E to 90° E. The corresponding data are represented on the right of fig. 1. Outside of this area, a constant ground elevation or zero is assumed. The rock depth is tracked from the crossing point up to an altitude of 7 500 m, which is slightly above Jengish Chokusu peak (7 439 m), the highest summit of Tian Shan. 1801×241 lines of sight have been scanned with azimuth and elevation values spanning $360 \times 12 \text{ deg}^2$.

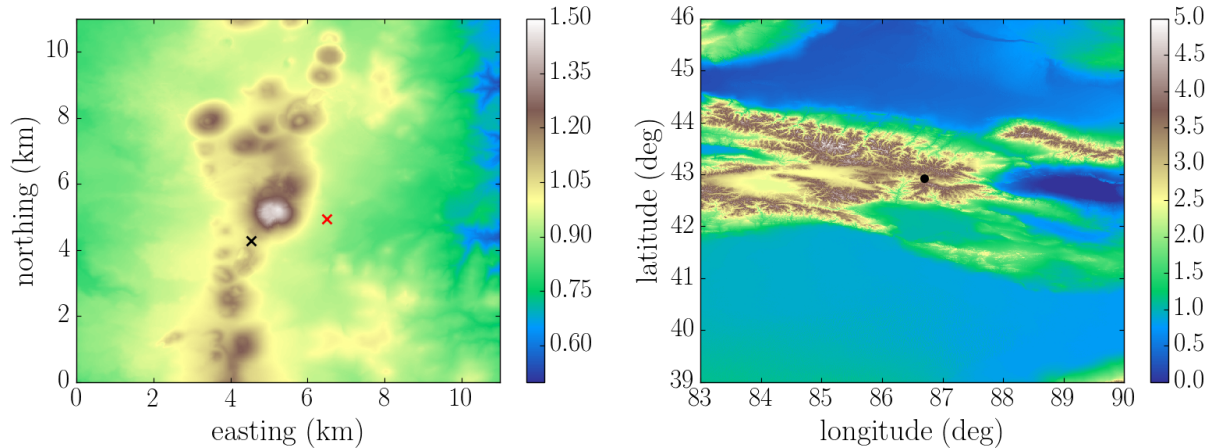


Figure 1: Elevation maps (km) of the case studies. Left: local map of the Chaîne des Puys (Lambert 93 projection). The black (red) cross indicates the CDC (TDF) location. Right: Tian Shan mountains. The black dot in the middle of the map indicates the location of the Ulatai valley.

5. Balancing speed and accuracy

The *optimistic* algorithm has two tuning parameters: the slope factor, α and the resolution factor, s_{\min} . In addition, TURTLE introduces a linear approximation, adding a third tuning parameter: the LLA range, r_{LLA} . These three parameters allow to balance accuracy versus speed, e.g. when computing the rock depth along a line of sight.

Estimating the accuracy of the computation is not as straightforward as it might first seem. Systematically setting small step lengths results in the accumulation of numerical rounding errors on large distances. For example, incrementing the position by steps of 1 cm results in a few mm deflection after 100 km, using an 8 bytes `double`. In the Ulatai view, this leads to errors of several meters on the rock depth for some peculiar trajectories that are grazing the ground. In the particular case of a straight line trajectory, this is solved by interpolating the step positions between the initial and

final location, instead of incrementing it by 1 cm. But in the general case this is not possible since the particle direction changes at each step.

For the present study, a *reference* set of rock depths is computed with a slope factor of $\alpha = 1\%$ and a resolution factor of $s_{\min} = 1\ \mu\text{m}$. No local approximation is used and the step position is interpolated along the straight line trajectory. This *reference* set is cross-checked against rock depths obtained with a constant initial step length of $s_0 = 1\ \text{cm}$ and interpolated positions as well. Note that the latter computation requires 20 CPU-days in the case of the full Ulastai view, with 217,921 lines of sight. Therefore, we do not use a step length lower than 1 cm. The *reference* case almost always produces identical results than the 1 cm case, while being $\times 100$ faster. In the few cases where differences are observed, decreasing the initial step length to $s_0 = 1\ \text{mm}$ for these specific trajectories shows that the *reference* case is correct against the $s_0 = 1\ \text{cm}$ computation. The rock depths computed with the *reference* case are shown on fig. 2. The typical value in the Chaîne des Puys area is a few km. In contrast, in the Ulastai valley, the visible rock depth can be above 100 km, close to the horizontal.

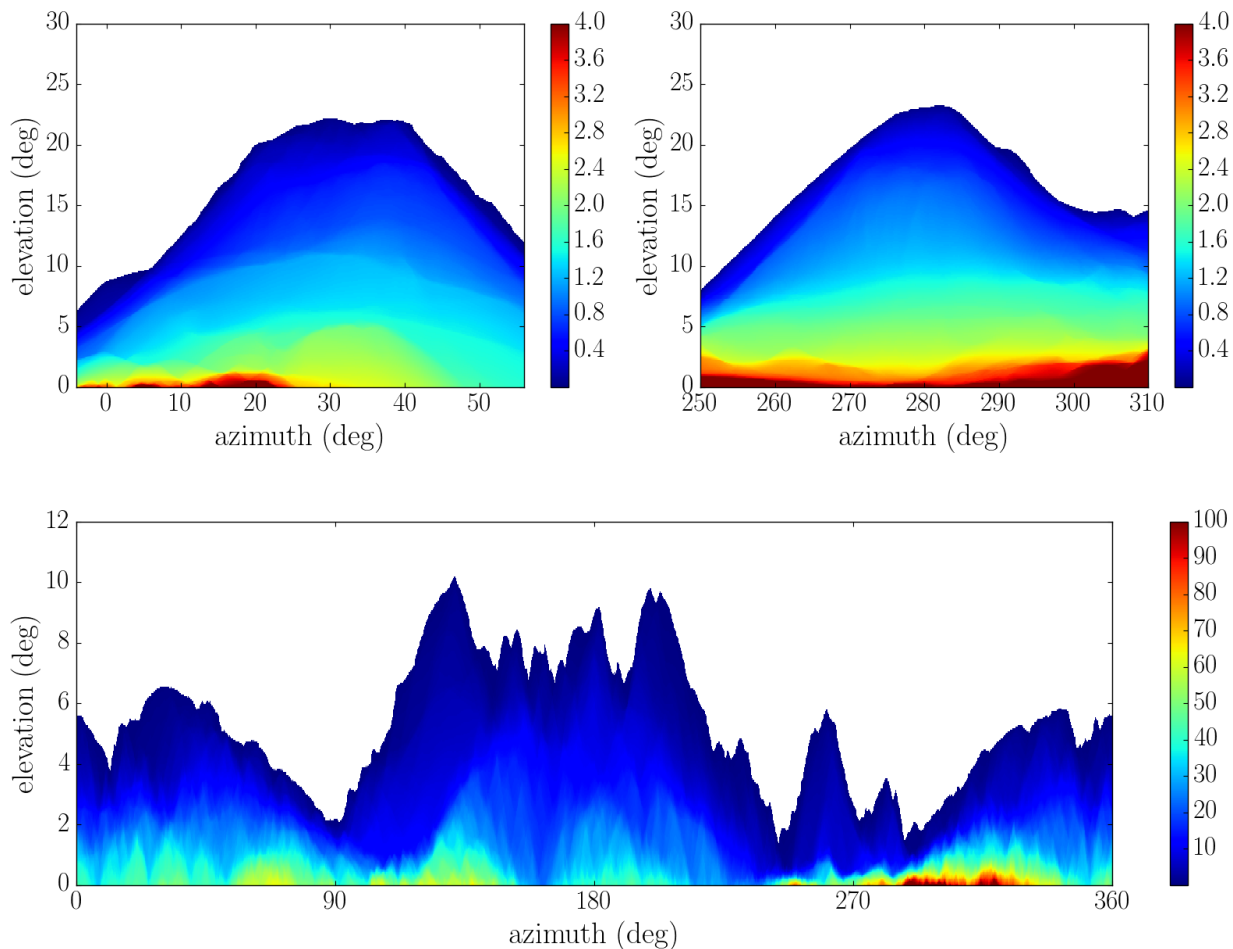


Figure 2: Rock depth (km) computed for various locations with the reference method. Top left: CDC view, Top right: TDF view, Bottom: Ulastai view. An azimuth of 0° points to the geographic north, and an azimuth of 90° points to the east.

We scrutinize the parameters of the stepping algorithm. The rock depth for the three views are computed for various parameter values using the `turtle_stepper_step` function. The track position is incremented step by step as it would be in a HEPMC. The absolute value of the difference, $|\Delta d|$, w.r.t. the *reference* result is taken as an estimate of the overrunning error on the rock depth, d . As a figure of merit we consider how the mean error varies as function of the mean CPU time, averaging over all lines of sight of a same view. Figure 3 illustrates how these criteria evolve when modifying the tuning parameters, one by one. Figure 3 corresponds to the CDC view, but similar results are obtained for the two other views. In the three cases, the following set of parameters yields a good compromise between speed and accuracy: $\alpha = 40\%$, $s_{\min} = 1$ cm and $r_{\text{LLA}} = 1$ m, as can be seen on figure 3. These parameters are located close to an inflection point. Reducing them below the selected value results in large cpu increase for little accuracy gain. For these parameter values, it is also cross-checked that interpolating the steps positions, rather than incrementing them, does not significantly reduce the error.

Figure 4 shows the error on the rock depth, $|\Delta d|$, for the selected parameter values. The mean of the error on the rock depth is low, 7 to 9 μm depending on the view. The sign of the error is positive in 50 % of the cases, i.e. there is an even probability to over or under estimate the distance. This is a strong result, since it shows that the *optimistic* algorithm, though error prone, is not biased. The magnitude of the discrepancy is only loosely correlated to the total rock depth: 10 % correlation factor for the TDF view, 5 % for the CDC one and 0.5 % for Ulatai. For the three views that we consider, with the selected parameters, all errors are below 1 cm *except* for one line of sight in the Ulatai view. For an observation angle of (55.4° N, 1.35° U) an error of 1.4 m occurs. Though, the relative error is of 49 ppm only. This problem is due to a very sharp peak, located at (43.093675° N, 87.038318° E), for which the last meter before the summit is cut through. Reducing the slope parameter to $\alpha = 0.2$ allows to resolve the top of this peak for horizontal trajectories, but this comes at the cost of a 81 % CPU increase.

A detailed look at individual tracks shows that the tail events, with errors of several mm, are due to trajectories grazing the topography, i.e. being almost parallel to some parts of the ground. These effects are visible on the error maps of Puy de Dôme (top plots of fig. 4). In particular, on the upper left plot (CDC view) one clearly sees details of the Puy de Dôme surface due to grazing rays. This effect is also visible on the upper right plot (TDF view). The top area of Puy de Dôme (above 10°) is very steep from this side. The lines of sight make a large angle with the slope of the volcano, and a good resolution is achieved. However, In the bottom area the slope is milder. As a result the lines of sight graze the ground smoothing out its roughness and leading to a poorer accuracy. It also explains the larger correlation observed between $|\Delta d|$ and the total rock depth. The Ulatai view is more complex since a single line of sight can stack several features: summits, valleys, etc ... The absence of correlation between $|\Delta d|$ and the total rock depth confirms that errors result from local peculiarities, e.g. a line of sight grazing a plateau, rather than from an accumulation of numerical errors.

The consumed CPU time for each line of sight is shown on fig. 5. Depending on the direction of observation, the CPU time varies by 2 to 3 orders of magnitude, from 10 μs to 10 ms. The CPU time increases abruptly when crossing rocks. The lines of sight crossing rocks, half of the total number, amount to 90 % of the CPU of a view. The CPU time is mainly driven by the rock depth, with correlation factors of 73 % (Ulatai), 77 % (TDF) and 87 % (CDC). The secondary factor is

the number of boundaries to map, i.e. the complexity of the topography. In addition, close to the horizontal, the CPU cost also increases due to the very long paths needed in order to reach the exit altitude, e.g. ~ 110 km at 0 deg of elevation in order to reach 2000 m high, starting from Col de Ceysat. The consumed CPU time is approximatively proportional to the number of Monte-Carlo iterations used in order to map a line of sight. The average ratio is of $0.5 \mu\text{s}$ per iteration for the Puy de Dome views.

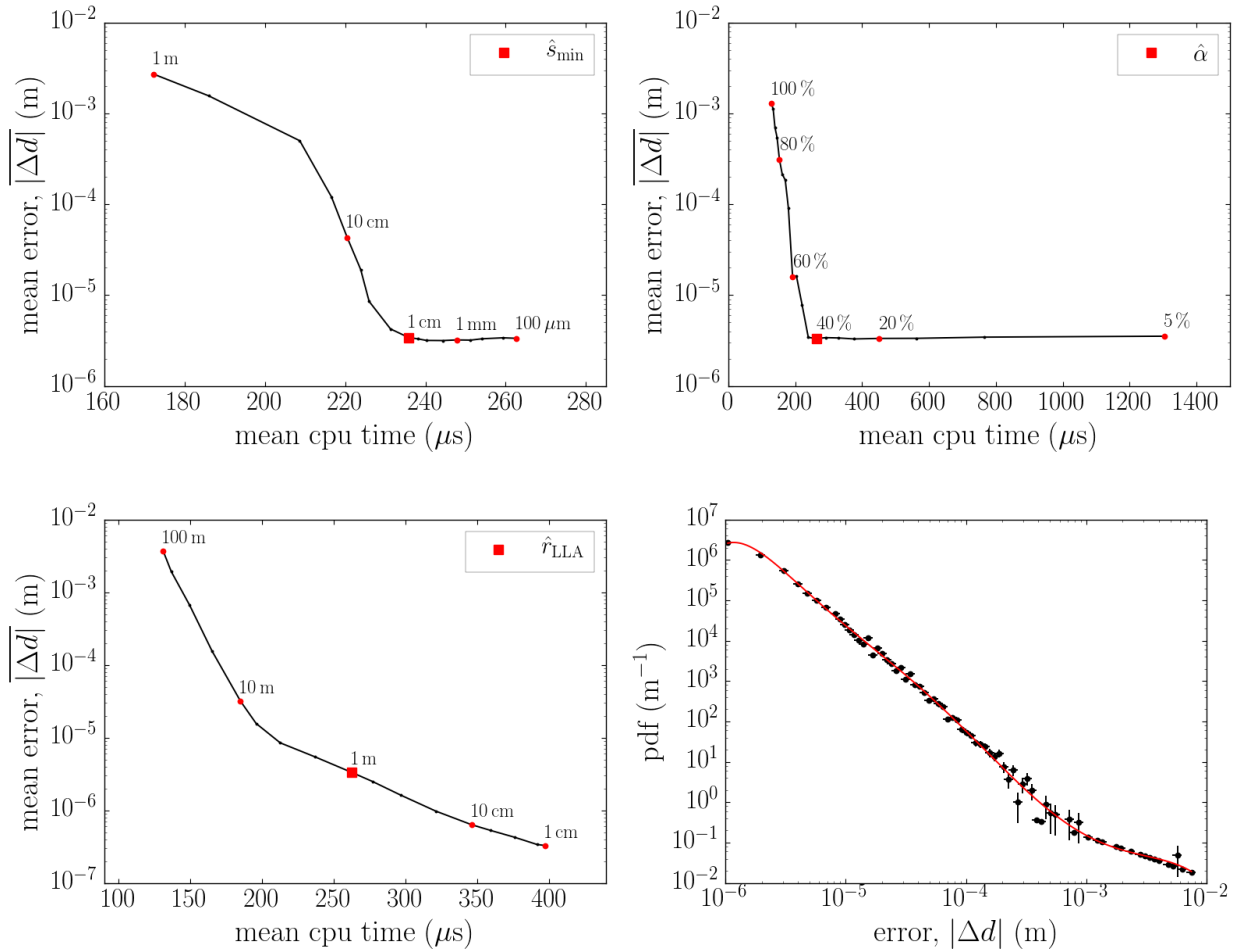


Figure 3: Accuracy versus CPU time for the CDC view, when moving the tuning parameters away from their selected value, indicated by a red square. Top left: variation with the resolution factor. Top right: variation with the slope factor. Bottom left: variation with the LLA range. Bottom right: error distribution for the selected parameter values ($\alpha = 40\%$, $s_{\min} = 1 \text{ cm}$, $r_{\text{LLA}} = 1 \text{ m}$).

6. Comparison with ray tracing algorithms

We compare the *optimistic* method discussed herein with the two alternative ray tracing algorithms discussed in the introduction: a BVH tree and a polyhedral mesh. In both cases the topography surface is modelled with triangular facets, joining the data nodes, and using ECEF coordinates. The

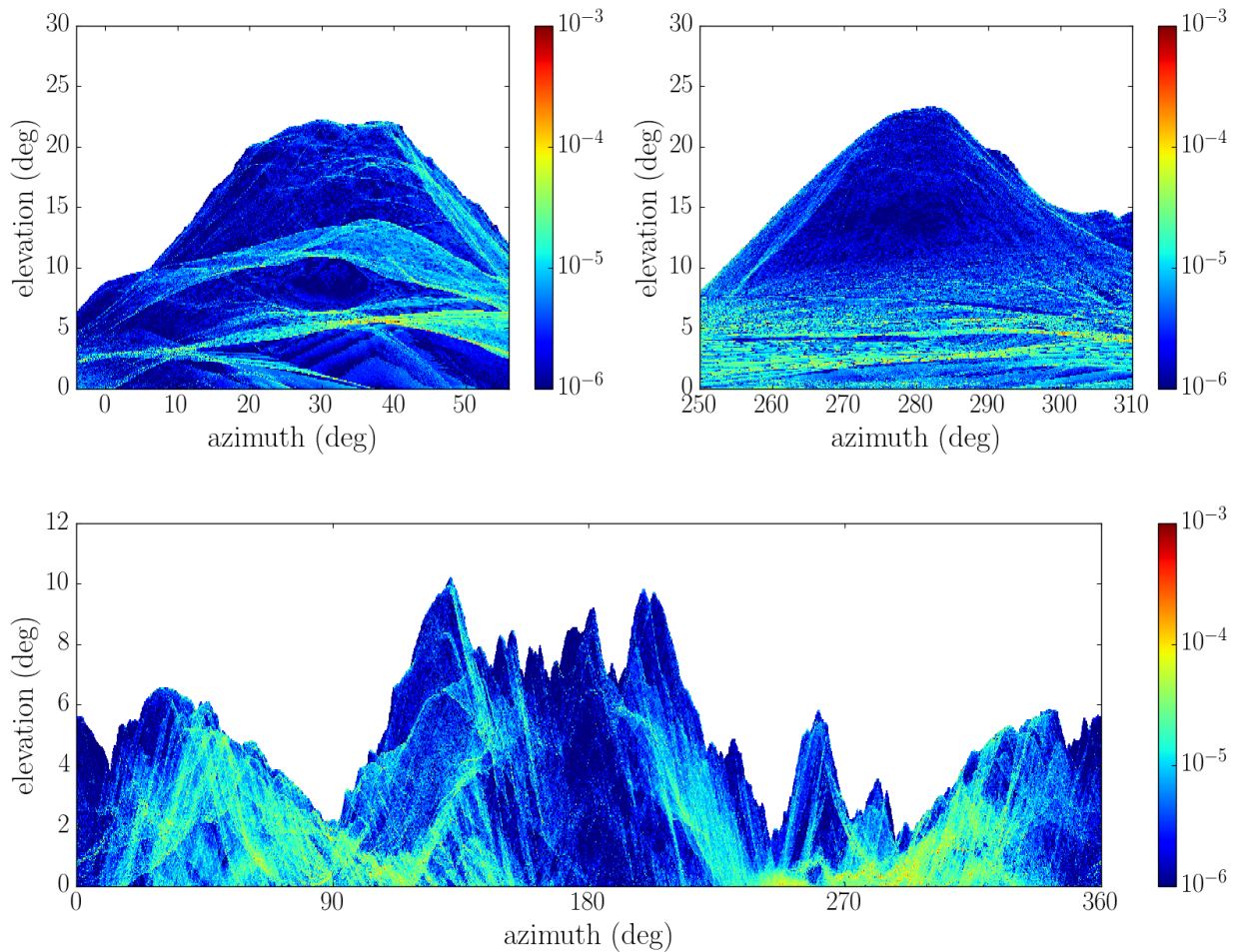


Figure 4: Error on the rock depth (m) with the selected parameter values: $\alpha = 0.4$, $s_{\min} = 1$ cm and a 1 m LLA range. Upper left: CDC view, Top right: TDF view, Bottom: Ulatai view. See fig. 1 for the site locations.

data nodes of a same grid are regularly spaced in geodetic or projected coordinates. Then, a square cell defined by four adjacent nodes is split in two triangular facets, dividing the bottom right and the top left of the cell, as illustrated on the left side of fig. 6. For the polyhedral mesh, the geometry is divided in 3D cells using triangular prisms. For each triangle of the tessellated topography surface we define a top (bottom) triangular prism, having the triangular facet as bottom (top) face. The sides of the prisms are all parallel, defined by the local vertical at the middle of the topography. The right side of fig. 6 shows a schematic of the top and bottom prisms of a triangular facet.

For the Chaîne des Puys views, the elevation data come from two different sources with different meshes. The inner mesh is inserted inside the outer one in ECEF coordinates, removing any outer node lying inside the inner mesh. Then, the *Triangle* library, from Shewchuk [22], is used in order to build the facets joining the border of the inner mesh to the outer one.

Tessellating a topography surface with triangles is a classical representation of a terrain. Let us recall that it differs from our approach which performs a bilinear interpolation of the terrain between

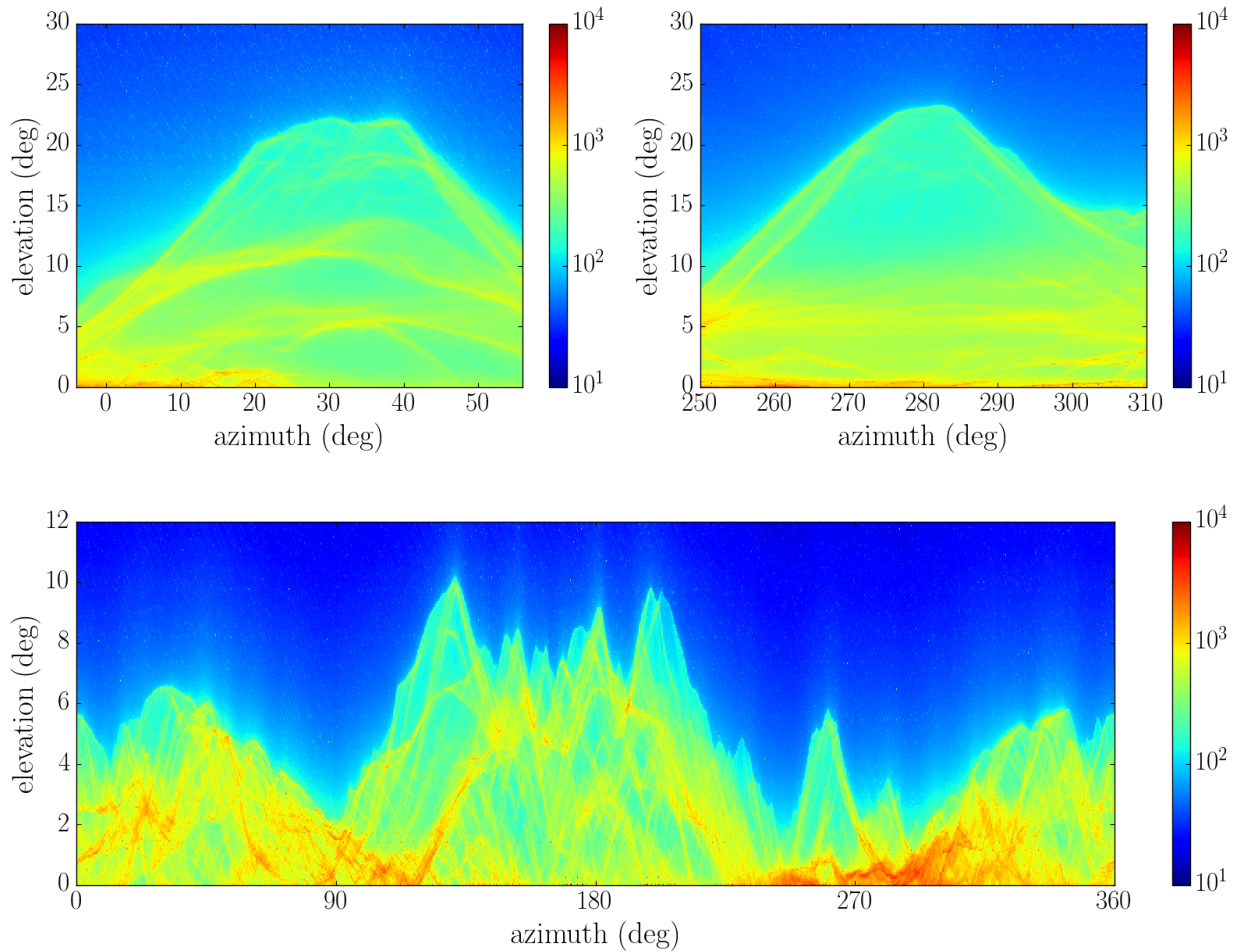


Figure 5: CPU time (μs) for computing the rock depth along a line of sight with the selected parameter values: $\alpha = 0.4$, $s_{\min} = 1$ cm and a 1 m LLA range. Upper left: CDC view, Top right: TDF view, Bottom: Ulastai view. See fig. 1 for the site locations.

nodes. As an example fig. 7 shows a vertical slice of the Chaîne des Puys topography modelled with the two methods. On a large scale no difference is visible (fig. 7, left). However, when zooming down to the grid resolution, discrepancies of several cm can be observed on the location of the ground between two grid nodes (fig. 7, right). For grazing rays, this can result in differences on the rock depth of the order of the spacing between grid nodes, i.e. several meters in this case.

Both competitor algorithms are implemented using the CGAL library [23] (v4.13) as well as the ECEF conversion and geographic projection routines from the TURTLE library. A `CGAL::Simple_cartesian<double>` Kernel is used. For the BVH method we use the generic AABB tree algorithm of Alliez et al. [24] with `CGAL::Triangle_3` primitives. The full geometry needs to be instantiated at the tree initialisation, resulting in a high memory overhead: 120 bytes per grid node. Once initialised, the `all_intersections` method of the `CGAL::AABB_tree` provide a fast computation of all intersections of the topography surface with a ray. However, the intersections with an AABB tree are not ordered w.r.t. to the ray origin. Therefore getting the closest intersection actually requires checking all intersections. Note that the `CGAL::AABB_tree`

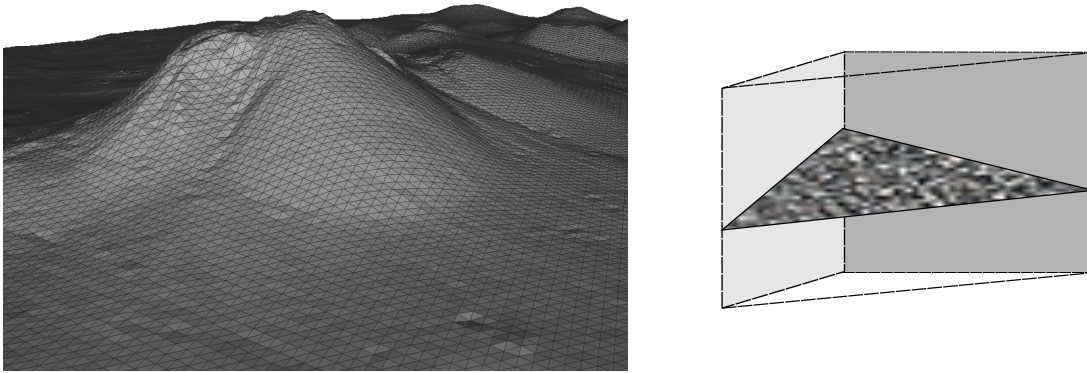


Figure 6: Tessellation of the topography data for the AABB tree and the polyhedral mesh algorithms. Left: tessellation of the ground surface using triangular facets joining the nodes. Right: schematic of a prism cell used for the tetrahedral mesh. The original triangular facet is the textured one.

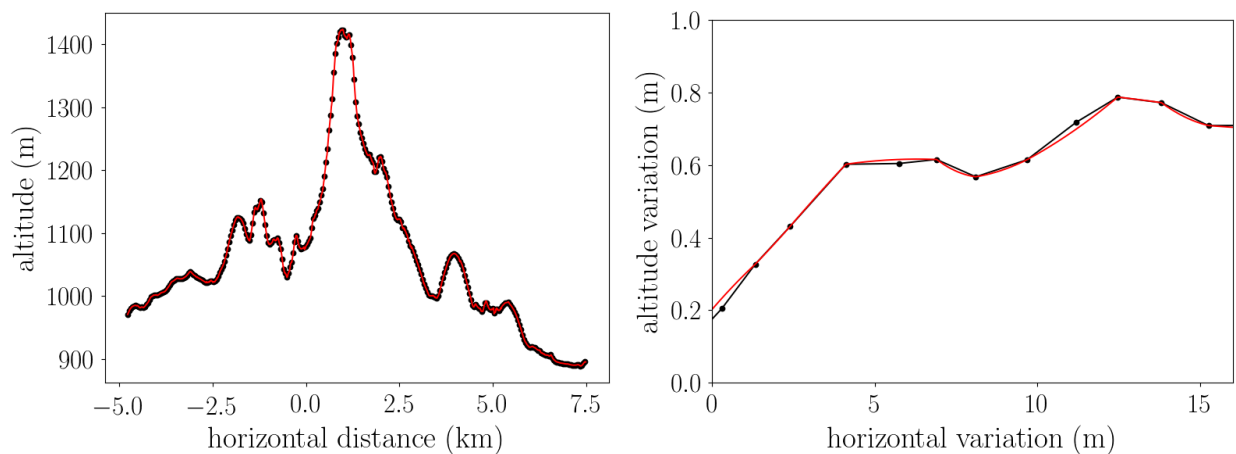


Figure 7: Vertical section of the inner topography data at an azimuth of 26° from the CDC site. Red: bilinear interpolation (TURTLE). Black: triangular facets (AABB tree and polyhedral mesh). The dots indicate the intersection points with the borders of individual facets. Left: full section but showing only one out of 30 facets intersections. Right: zoom at an horizontal distance of 880 m.

has a `first_intersection` method since v4.9. However it was found to be significantly slower ($\sim 2\times$) than manually looping over the result of `all_intersections`.

For the polyhedral mesh, a `CGAL::Plane_3` object is used in order to represent the prisms facets, positively oriented towards the outside of a cell. The `CGAL::Plane_3::has_on_positive_side` method allows to test if a point lies on the inner or outer side of a facet. Since a triangular prism is a convex shape, a point is located inside if and only if it is on the inner side of all of its facets. Using triangular prisms instead of tetrahedra allows to reduce the total number of facets to test when navigating through the geometry. The

total memory usage is kept low by creating and destroying the prisms on the fly from the raw topography data.

The rock depth along a line of sight is computed following pseudocode 1. In the case of the BVH algorithm the `volume_at` function is implemented by counting the number of intersections of a vertical ray with the topography surface. An even number of crossings implies that the initial position is below the tessellated ground. Then, the `distance_to` function proceeds by locating the closest intersection with a ray along the line of sight. The intersection points define segments. The rock depth is computed from the length of the segments lying below the surface. Note that in this particular case where trajectories are straight, it is more efficient to map all intersections with the AABB tree in a single step, since we get all of them by default. For the purpose of this comparison, both methods are implemented for the AABB tree, i.e. getting all intersections in a single row, or stepping from one to another as in a HEPMC.

For the polyhedral mesh, the `volume_at` function proceeds in two steps. First we locate the closest grid node using geodetic or projected coordinates. Then we test the prisms connected to this node. Once the initial volume is located, we step through the prisms and locate the intersections with the top or bottom faces. Note that since the prisms are connected by their faces there is no need to re-locate the next prism when exiting the current one. The exit face determines the next sub-volume.

Fig. 8 shows the differences on the computed rock depths, $|\Delta d|$, when using triangular facets or a bilinear interpolation of the DEM data. A striking feature is that these differences are much larger than the overrunning errors of the tuned *optimistic* method (fig. 4). For the CDC and TDF views the average absolute difference is 12 cm and 8 cm respectively. For the Ulastai view the average value is ten times higher: 118 cm. This result is consistent with the fact that the grid spacing is ten times larger for the SRTMGL1 data than in the inner grid used for the Chaîne des Puys. The sign of the difference is evenly distributed in all three cases. The distribution of the absolute difference is shown on the right of fig. 9. It reflects the vertical differences of the topography in both models, shown on the left of the figure. The extreme values of $|\Delta d|$ are consistent with the respective spacing between grid nodes.

The performances of the three algorithms are compared by varying the number of nodes of the DEM data. A periodic down sampling is applied in order to vary the number of nodes. For the Puy de Dôme data, by convenience, only the inner grid is used for this study. We record the CPU time and the number of Monte-Carlo iterations for each line of sight. The upper part of fig. 10 shows the average CPU time per line of sight as function of the number of nodes. For the BVH algorithm intersections are computed in a single row. Clearly, the AABB tree performs the best when it only comes to map all intersections of the topography with a straight ray. Though, for the full Ulastai data 200 GB of RAM are needed. As a result the test server needs to use its swap memory, resulting in a slow down by a factor of ten in the full map case. In addition, when the geometry has more than $n = 10^7$ nodes, the initialisation of the AABB tree requires more time than scanning all the $\sim 200,000$ lines of sight.

In comparison, the polyhedral mesh algorithm is not efficient for intersecting large grids. Its CPU time is fitted with a square root law: $a + b\sqrt{n}$, in agreement with expectations. For the AABB tree the increase rate is found to follow a power law: an^b , with an exponent of $b = 1/8$. Interestingly, the performances of the *optimistic* algorithm do not depend on the number of nodes, but only on the ray length and the topography features. As a result it outperforms the polyhedral mesh for grids

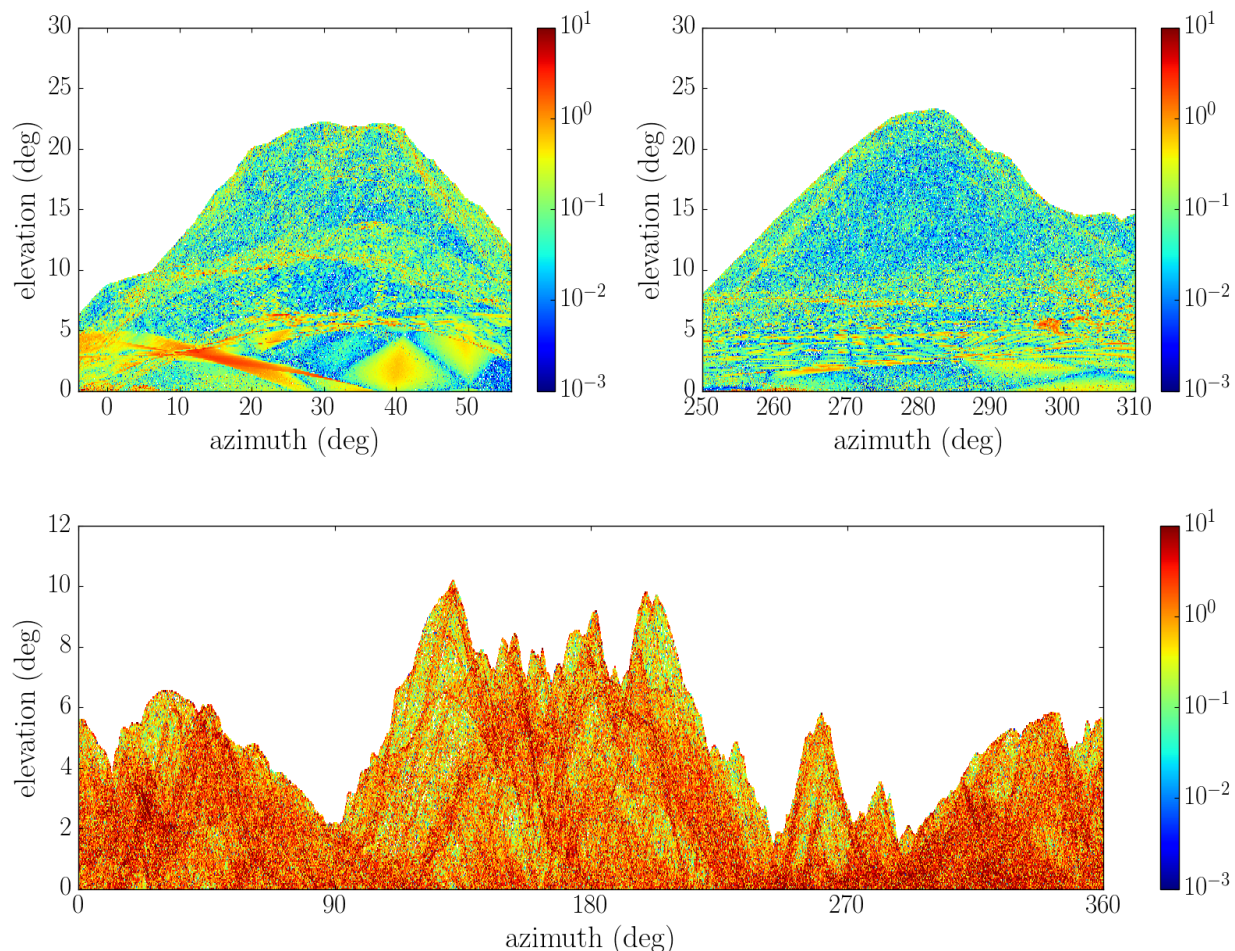


Figure 8: Differences on the rock depth (m), Δd , between triangular facets and a bilinear interpolation. Upper left: CDC view, Top right: TDF view, Bottom: Ulastai view. See the text for the exact site locations.

larger than 1000×1000 nodes. In principle it should also be faster than the AABB tree for extreme grid sizes. But, the large amount of memory required by the AABB tree is likely to be an issue before this ever happens.

In the case where the step sizes are limited by the physics, the relevant parameter is the average CPU time spent at each HEPMC step in order to resolve the geometry. An estimate of this quantity is provided by the total CPU time for all lines of sight of a view divided by the total number of transport iterations. This parameter is indicated on the lower part of fig. 10. In this configuration the AABB tree algorithm is inefficient. The *optimistic* algorithm performs best. It is a hundred times faster than the BVH algorithm, for large grids. The polyhedral mesh is two (six) times slower than the *optimistic* algorithm, for the Ulastai (CDC) view. However, the present comparison of the polyhedral versus *optimistic* algorithm should be considered with precaution. The CPU time per step can vary strongly in both cases, depending on the step length dictated by the physics. In the Polyhedral case, the first step in a prism is much longer than the subsequent one, since the local geometry needs to be built. A closer analysis, using valgrind [25] & callgrind [26], shows that

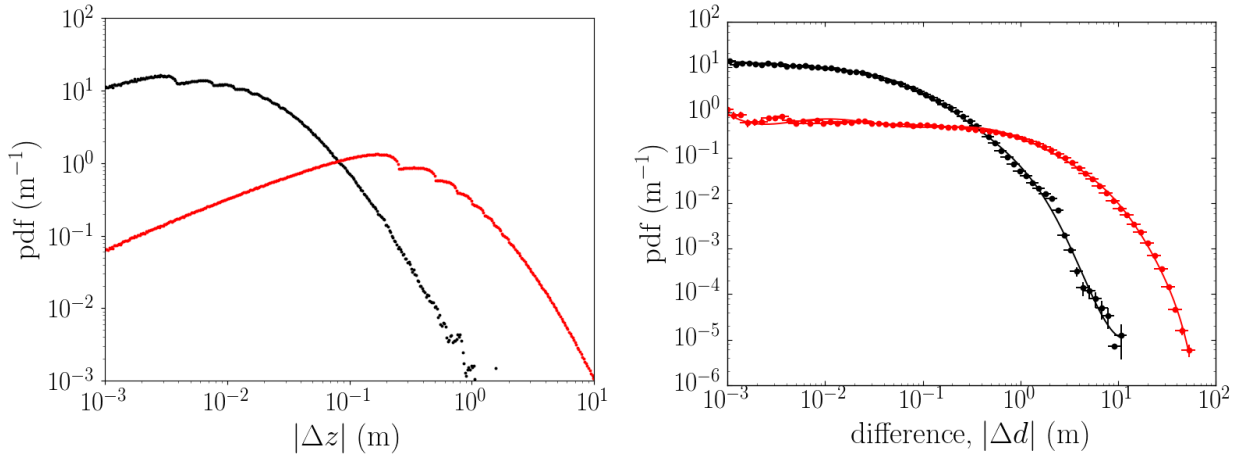


Figure 9: Distribution of the absolute differences, in meters, when using triangular facets or a bilinear interpolation. Red: Ulatai view. Black: CDC view. Left: distribution of the vertical difference. Right: distribution of the difference on the rock depth.

building the prisms on the fly represents 75% (Ulatai) to 93% (CDC) of the CPU instructions of a Monte-Carlo step, with our implementation. In the present study each prism is traversed in a single step, which is the worst case. Similarly, for the *optimistic* algorithm, depending on the set LLA range, successive small steps are accelerated by TURTLE.

Looking back at fig. 10, one might wonder why for the polyhedral mesh, the CPU time is five times larger in the CDC view than in the Ulatai one. A detailed analysis with callgrind shows that this is due to the fact that the Chaîne des Puys inner map uses Lambert 93 projected coordinates, whose conversion has a high CPU cost: six times more instructions than when using geodetic coordinates. As a result, building the prism geometry is very inefficient. This could be solved by re-meshing the elevation data in geodetic coordinates, or even better, directly in a plane projection in ECEF coordinates. The *optimistic* algorithm uses a TURTLE stepper with a 1 m LLA range. It mitigates the CPU overhead introduced by the map projection. As a result, the CPU time is only two times larger in the CDC view than in the Ulatai one.

7. Performances in HEPMC simulations

When integrated in a HEPMC, the *optimistic* method introduces a slow-down w.r.t. to the sole physics processing. This slow-down arises from two factors. First, computing the geometric step length adds an extra CPU cost at each Monte-Carlo step. This factor is common to all geometry navigation methods. The *optimistic* and polyhedral mesh methods are designed in order to minimise this cost. However, they add a second slow-down factor by increasing the total number of Monte-Carlo steps required for the navigation through the geometry. Depending on the CPU cost of each step, and the number of added steps, limiting the geometric step length might be worth or not.

In order to check the performances of the TURTLE library, when integrated in a HEPMC, let us consider a classical problem for muography applications: the computation of the atmospheric μ

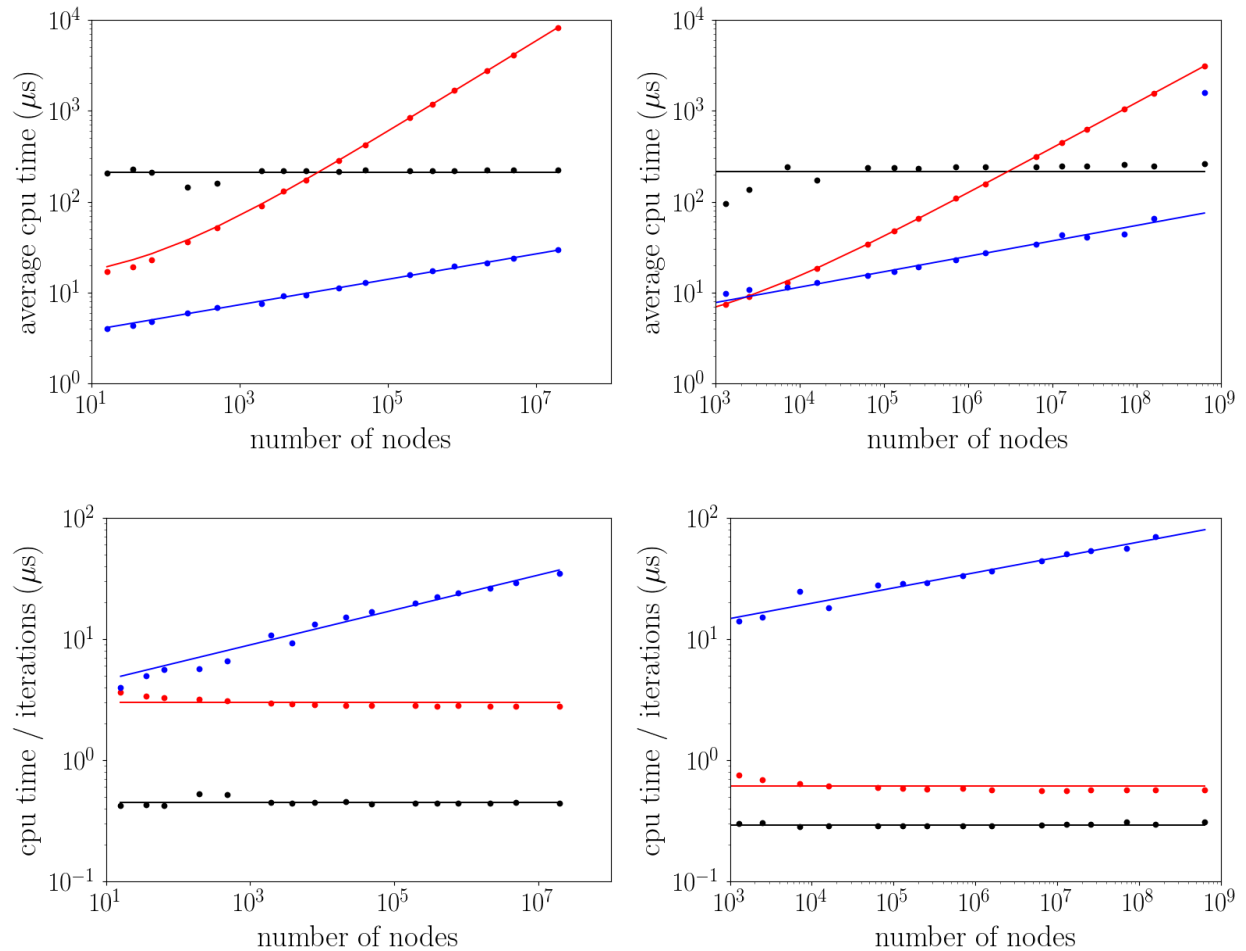


Figure 10: CPU time (μs) as function of the number of grid nodes. Black: *optimistic* algorithm. Red: polyhedral mesh. Blue: BVH tree. The solid lines correspond to fit model described in the text. Upper: average CPU per line of sight for the CDC (left) and Ulastai (right) views. Bottom: CPU per Monte-Carlo iteration for the CDC (left) and Ulastai (right) views.

flux for each line of sight of the three views previously considered. Such a problem is efficiently solved using a reverse Monte-Carlo method, where the particles are tracked backward from the detector to the source. The PUMAS [17] library provides a backward Monte-Carlo engine for μ or τ . Details of the backward method can be found in Niess et al. [27]. For the present study, version 0.12.p01 of PUMAS is used, together with a `turtle_stepper`. A minimal example of geometry callback for PUMAS, using TURTLE, is provided in appendix A. The short mode of the stepper is used, i.e. requiring only the *optimistic* stepping distance. Indeed, PUMAS transport engine natively accepts both exact and approximate geometric step lengths. When a change of medium occurs, PUMAS locates the medium boundary with a binary search, if not already on a boundary.

Note that the TURTLE library and its *optimistic* stepping scheme can also be integrated in a generic Monte-Carlo like Geant4, without modifying the base engine. This is further discussed in Ap-

pendix B. However, for the present study it is clearer to use a less complex Monte-Carlo engine like PUMAS.

For each line of sight, the μ spectrum is estimated by backward sampling 100 μ . The μ final kinetic energy is randomised over a $1/E$ distribution between 1 MeV and 1 PeV. Note that *a priori* any distribution could be used for the final kinetic energy, as long as it covers the full range of possible values. Using a $1/E$ distribution is a good pick for this problem, reducing the Monte-Carlo variance. It amounts to drawing the logarithm of the final kinetic energy from a uniform distribution. The particle is then positioned at the start of the line of sight, oriented along the line. From there on it is backward transported until it reaches the primary source, above, or until it escapes the simulation area by the sides. The primary source is set at an altitude of 2 000 m (CDC and TDF) or 7 500 m (Ulastai), as for the ray tracing problems. The maximum kinetic energy of the primary μ source is set to 100 PeV. Above this energy the atmospheric μ flux is too low, for muography applications. Whenever a backward propagated μ exceeds this energy the track is stopped.

The Monte-Carlo is run with two different levels of detail for the physics. In the first mode, an *hybrid* simulation is done. The μ energy loss processes are split in a soft and in a hard component. The soft component is dominated by μ ionisation losses. It constitutes the bulk of the energy loss, for μ with energies below 1 TeV. This component is approximated as purely deterministic. The hard component is dominated by catastrophic radiative processes: μ *Bremsstrahlung* and e^+e^- *Pair creation*. For those, a detailed stochastic treatment is applied. In addition, transverse scattering is not simulated, in particular Coulomb multiple scattering is disabled. These assumptions are usual for the transport of high energy μ , see e.g. Sokalski et al. [28]. The hybrid mode provides a fast, yet accurate, computation of the μ flux transmitted through tens of meters of rocks, or more. In the second mode, a *detailed* simulation is done, enabling all physics processes. This mode is required for accurate estimates of the low energy flux ($E \leq 10$ GeV) of scattered atmospheric μ . Note that PUMAS actually allows to switch the level of detail of the physics on the fly, during the tracking of a particle. An efficient strategy is to switch from a detailed transport to an hybrid one as the μ energy increases, during its backward transport. Nevertheless, for the sake of clarity we consider both modes separately in the present study.

The PUMAS library is hacked by overriding transverse deflections to zero, such that, whatever the physics mode, all particles follow a straight trajectory along the line of sight. Note that the hack is applied after computing any deflection angle, in order to properly count the corresponding CPU cost. Forcing all particles to follow the line of sight, i.e. to encounter exactly the same distribution of matter, allows for a rigorous comparison of performances. In addition, it allows to pre-compute the geometry in all cases, using a ray tracing algorithm. Then, the distance to the next boundary can be very quickly inferred from the μ distance to the start of the line of sight. Using this geometry mode provides an estimate of the CPU cost of the bare physics, subtracting the CPU cost for the geometry pre-computation.

The CPU cost for the physics simulation depends on the μ final energy. The lower the μ energy the shorter the physical steps and the higher the corresponding CPU cost. The CPU cost also increases in rocks since the physical steps length decreases by 3 orders of magnitude, due to the differences in target density. This is counterbalanced by the fact that the μ path length in air, up to the primary

altitude, is larger than in rocks. Averaging over all lines of sight and μ energies, the CPU cost is dominated by low energy particles escaping from rocks.

Table 2 shows a summary of the mean performances per line of sight for the various HEPMC configurations, as well as for the sole ray tracing problem. Considering the physics only, in hybrid mode a μ can cross the whole simulation area in a single Monte-Carlo iteration in air, and in a dozen of iterations when the line of sight intersects rocks. In detailed mode hundred times more iterations are needed, due to the simulation of the multiple scattering and of the fluctuations in the ionisation loss. In comparison, the ray tracing with the *optimistic* method requires ~ 100 iterations in air and 1 000 to 2 000 through rocks.

The previous numbers show that in hybrid mode the simulation is limited by the ray tracing. The mean CPU time per line of sight is close to the one obtained for the ray tracing, though 16 % (Ulastai) and 50 % (CDC & TDF) higher because of the extra cost of the physics at each Monte-Carlo step. This was confirmed using *valgrind* & *callgrind*. The physics amounts to 36 % (CDC & TDF) and 54 % (Ulastai) of the total CPU instructions for hybrid simulations. The higher cost of the physics in the Ulastai view is consistent with the fact that the geometry cost per Monte-Carlo iteration is two times lower than in the Chaîne des Puys views, because of the cartographic projection, as seen in section 6. Figure 11 shows the *slow-down* w.r.t. the ray tracing, defined here as the ratio of the CPU time in hybrid mode to that of the ray tracing. For the Chaîne des Puys views the slow-down is rather uniform. For the Ulastai view the results are more contrasted. Because of the higher relative CPU cost of the Physics, one would expect higher slow-downs than for the Chaîne des Puys views. This is indeed observed for the line of sights in the sky area, i.e. that do not cross the topography. However, the hybrid simulation appears to be faster than the sole ray tracing at large rock depths. This is due to the fact that the tracking is stopped before reaching the primary altitude, as the μ kinetic energy exceeds 100 PeV. This explains the more contrasted results in intermediary regions. Since, the line of sights crossing rocks dominate the total CPU cost, it also explains why the mean CPU time in the Ulastai case is closer to the ray tracing one, despite the relative physics cost being higher.

In detailed mode, the bulk of the CPU is spent in the physics simulation. The geometry amounts only to 15-20 % of the total CPU. This is consistent with the fact that in detailed mode the CPU needed for the bare physics simulation is 4 times larger than the one for the ray tracing, as can be seen in table 2. The ray tracing doesn't increase significantly the number of Monte-Carlo iterations, in detailed mode: by a factor 2 (CDC & TDF) and 4 (Ulastai). In comparison, in hybrid mode the increase is of $\mathcal{O}(100)$. As a result, the total CPU time is similar to the one needed for the bare physics simulation, only a factor of two higher. Locally, higher slow-downs (5-6, w.r.t. the physics) can occur, for grazing rays, as can be seen on fig. 12. In such cases, the number of Monte-Carlo iterations increases by one order of magnitude.

From the results collected in table 2 and in previous section 6, we can estimate the HEPMC performances that one would achieve when using an AABB tree or a Polyhedral mesh for the geometry navigation. In the case of the Polyhedral mesh the total traversal time of the topography would limit the HEPMC performances, both in hybrid and detailed mode. The ray tracing requires more than 10 ms for the Chaîne des Puys views and 3 ms for the Ulastai one. This is already higher than what is achieved for the detailed HEPMC simulation, 2 ms, using the *optimistic* algorithm. There-

View	Configuration		Mean CPU time (μs)	Mean iterations	
				Air	Rock
CDC	Ray tracing		247	90	849
	Hybrid	physics	21	1	11
		all	374	90	854
	Detailed	physics	966	101	484
		all	1 832	157	1 155
TDF	Ray tracing		285	86	901
	Hybrid	physics	24	1	12
		all	425	86	905
	Detailed	physics	983	104	502
		all	1 990	156	1 182
Ulastai	Ray tracing		286	111	1 721
	Hybrid	physics	50	1	37
		all	334	111	1 080
	Detailed	physics	1 082	208	581
		all	1 815	259	1 447

Table 2: Mean statistics for various HEPMC configurations and for the ray tracing using the *optimistic* algorithm. The mean CPU time and the mean number of Monte-Carlo iterations are averaged per line of sight.

fore, a Polyhedral mesh is not competitive in this situation. It would be competitive for smaller mesh sizes however, with $\sim 10^5$ nodes or less.

For the AABB tree, the total traversal time is very fast on the contrary. Assuming that Random Access Memory (RAM) is sufficient, one can extrapolate the models found in section 6, for the AABB tree, to the total number of nodes. It yields a mean CPU time per line of sight of $35 \mu s$ (CDC) and $75 \mu s$ (Ulastai). Adding up the CPU time needed for the bare physics, in hybrid mode the mean CPU time would be of $\sim 60 \mu s$ (CDC) and $125 \mu s$ (Ulastai), for the AABB tree. This is a factor of 2 (Ulastai) and 5 (CDC) speed-up w.r.t. the *optimistic* algorithm. In detailed mode however, a full ray tracing would be done at each physical Monte-Carlo step, since the particle direction changes. Then, the mean CPU time would be of 12 ms (CDC) or 45 ms (Ulastai) per line of sight. This would be one order of magnitude higher than what is achieved with the *optimistic* algorithm. For muography applications one actually needs to run a mixed simulation, using both detailed and hybrid mode. In this situation, the total CPU time is dominated by the detailed simulation of low energy particles. Hence, the AABB tree would not be competitive in this case. It could however bring a moderate speed-up ($\times 2$ at most) for neutrinos transport over large scales. But this comes with a high memory cost of $\mathcal{O}(100)$ GB, requiring to run on dedicated hardware.

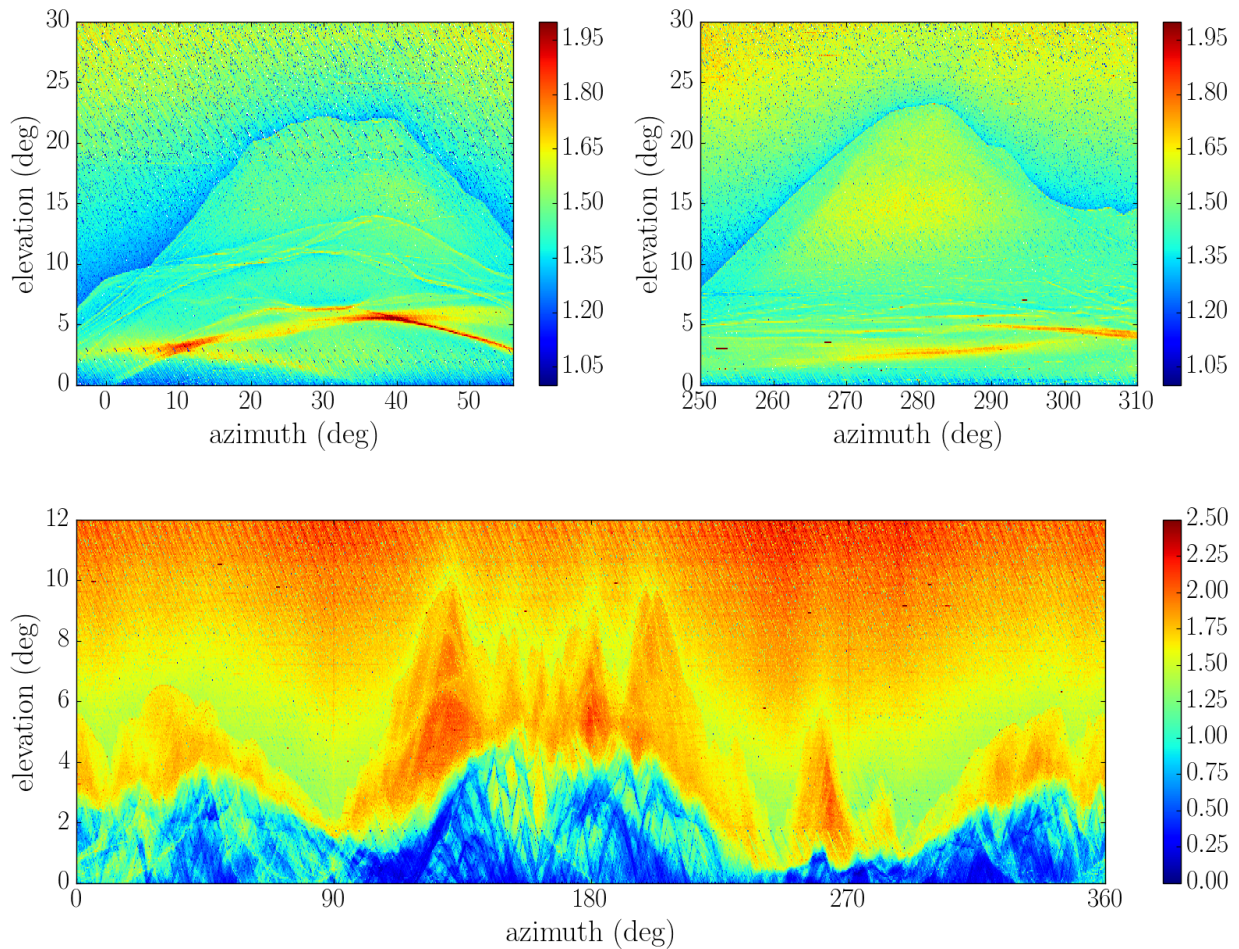


Figure 11: Slow-down factor when computing a μ spectrum with PUMAS in hybrid mode. The slowdown is w.r.t. to the ray tracing. Upper left: CDC view, Top right: TDF view, Bottom: Ulas-tai view.

8. Conclusion

The *optimistic* method is a fast and efficient method for navigating through topographies. Contrary to traditional ray tracing methods, the *optimistic* method proceeds by trials and errors. It takes the risk of overrunning some details of the geometry. In the case of a topography described by a DEM, this risk can be efficiently controlled by adapting the stepping distance as a function of the height above ground. Using this strategy, errors are kept below the native accuracy of DEM data. In addition, the *optimistic* method naturally handles higher interpolation models between the grid nodes than the traditional flat triangular facets. Differences on the rock depth of the order of the distance between the grid nodes can be observed, when using a triangular tessellation or a bilinear interpolation.

A dedicated library is implemented in C: TURTLE. It provides utilities for navigating through a topography described by a DEM, using the *optimistic* method. The elevation data of a DEM are encapsulated in `turtle_map` objects. Values between nodes are rendered with a bilinear in-

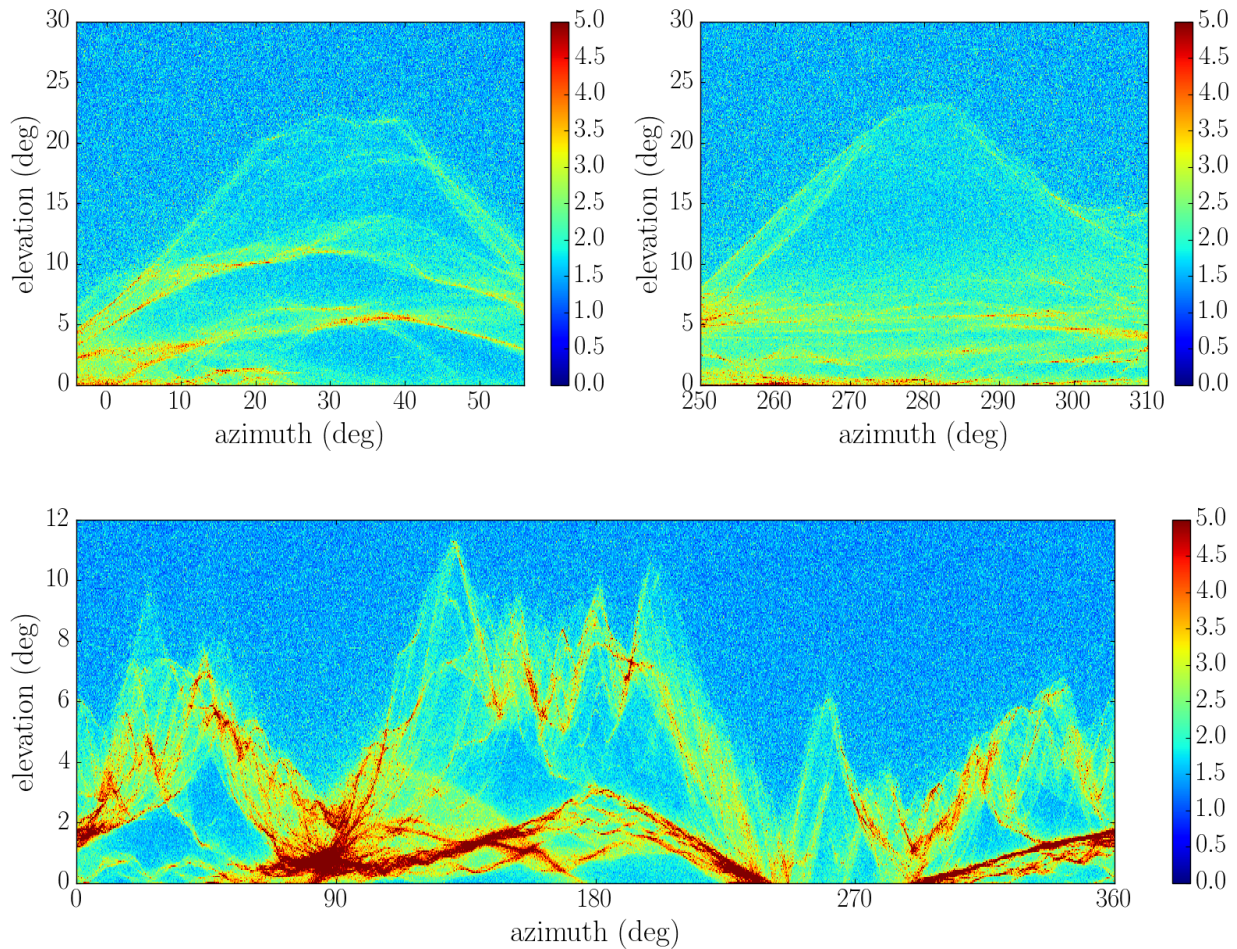


Figure 12: Slow-down factor when computing a μ spectrum with PUMAS in detailed mode. The slowdown is w.r.t. to the physics only. Upper left: CDC view, Top right: TDF view, Bottom: Ulatai view.

terpolation. Collections of maps, as provided by global DEMs for example, are managed with `turtle_stack` objects. The `turtle_client` object provides thread safe access to stacks of maps. TURTLE supports a few cartographic projections, including UTM. The TURTLE library also provides transforms for representing the topography data in Cartesian ECEF coordinates. The top level component of the library is the `turtle_stepper` object. It provides navigation functionalities.

The traversal time of the *optimistic* method does not depend on the number of nodes of the DEM grid, contrary to other methods. It only depends on the extent of the topography, and on its details. The more a ray is grazing the ground, the longer its traversal time. In addition, the *optimistic* method was implemented in TURTLE with zero extra memory cost, apart from the initial DEM data. Thus, this method performs particularly well for large grids, with more than 10^9 nodes. In such cases, an AABB tree is only three times faster while requiring $\mathcal{O}(100)$ GB of extra memory. Polyhedral meshes are not competitive for large scales.

The *optimistic* method is most efficient when navigating through a topography in detailed HEPMC simulations. Applied to a muography Monte-Carlo, the TURTLE library allows to render a large scale topography on the fly while only slowing down the simulation by a factor of two, w.r.t. the bare physics. This is due to the fact that the *optimistic* method provides both fast estimates of the distance to the ground together with a fast traversal time. Fast estimates are required in order to efficiently track particles that frequently change direction. Tree like geometry optimisations are not well tailored for such cases, because they perform a full ray tracing at each Monte-Carlo step.

The current implementation based on eq. (1) could be further refined. A simple improvement would be to vary the slope parameter, α , depending on the map region. For example in plain regions, values of α larger than in mountainous areas could be used. This would however require a preliminary analysis of the map data. The algorithm discussed in this paper is already very efficient, despite being extremely simple. It has no memory overhead and requires no initialisation, apart from loading the initial DEM data.

Acknowledgements

This research was financed by the French Government Laboratory of Excellence initiative no. ANR-10-LABX-0006, the Region Auvergne, the European Regional Development Fund and the France China Particle Physics Laboratory. This is Laboratory of Excellence ClerVolc contribution number XXX. The SRTMGL1 (v3) topographical data used in this study were retrieved from the online USGS EarthExplorer and NASA Earthdata Search tools, courtesy of the NASA EOSDIS Land Processes Distributed Active Archive Center (LP DAAC), USGS/Earth Resources Observation and Science (EROS) Center, Sioux Falls, South Dakota.

A. Example of a TURTLE topography in PUMAS

```
#include <stdlib.h>
#include "pumas.h"
#include "turtle.h"

/* Limits of the geometry */
#define ALTITUDE_MIN -11E+03
#define ALTITUDE_MAX 9E+03

/* Set a uniform density for the atmosphere */
static double locals_air(struct pumas_medium * medium,
    struct pumas_state * state, struct pumas_locals * locals)
{
    locals->density = 1.205;
    return 0.;
}

/* Set a uniform density for rocks */
static double locals_rock(struct pumas_medium * medium,
    struct pumas_state * state, struct pumas_locals * locals)
{
    locals->density = 2.65E+03;
    return 0.;
}
```

```

}

/* List of propagation media */
static struct pumas_medium media[2] = {
    { .material = 1, .locals = &locals_air },
    { .material = 0, .locals = &locals_rock }};

/* TURTLE stepper object, for navigating the topography */
static struct turtle_stepper stepper = NULL;

/* Callback for locating the current medium */
static double medium(struct pumas_context * context,
    struct pumas_state * state, struct pumas_medium ** medium_p)
{
    /* Get an optimistic step length from TURTLE */
    int layer;
    double altitude, ground, step;
    turtle_stepper_step(stepper, state->position, NULL, NULL,
        NULL, &altitude, &ground, &step, &layer);

    if ((layer < 0) || (altitude < ALTITUDE_MIN) ||
        (altitude > ALTITUDE_MAX)) {
        /* The particle has escaped the geometry */
        if (medium_p != NULL)
            *medium_p = NULL;
        return 0.;
    } else {
        /* Update the current medium */
        if (medium_p != NULL)
            *medium_p = (altitude > ground) ?
                media : media + 1;
        return step;
    }
}

int main(int argc, char * argv[])
{
    /* Initialise the TURTLE stepper and configure it */
    turtle_stepper_create(&stepper);
    turtle_stepper_add_flat(stepper, 0.);

    struct turtle_stack * stack;
    turtle_stack_create(
        &stack, "path/to/data", 0, NULL, NULL);
    turtle_stepper_add_stack(stepper, stack);

    /* Clean TURTLE objects and exit */
    turtle_stepper_destroy(&stepper);
    turtle_stack_destroy(&stack);

    exit(EXIT_SUCCESS);
}

```

B. G4Turtle

The `G4Turtle` class provides an example of interfacing of the TURTLE library with Geant4. It encapsulates a `turtle_stepper` object and its related data: `turtle_map`, & `turtle_stack`. The source code is available from GitHub [29] under the LGPL-3.0 license. The `G4Turtle` interface is provided as a demonstration that the TURTLE library can be integrated in a generic Monte-Carlo like Geant4, without modifying the base engine. We do not claim that the present implementation is the most genuine one. In particular, it doesn't support multi threading and it requires disabling the `SmartVoxels` navigation at the topography level. It is functional though, with a mild CPU slow-down per Monte-Carlo step.

In Geant4 a geometry is described by a set of volumes bounded by `G4VSolid` objects, e.g. `G4Box`, `G4Orb`, ... and filled with `G4Materials`. These volumes are ordered by inclusion relations. The top volume is called *World*. Each `G4VSolid` implements in particular the `Inside`, `DistanceToIn` and `DistanceToOut` methods. These methods allow to check if a particle is inside or outside of the volume, and to compute the distance to the volume border, following a straight line along the particle direction. Note that for these later methods, Geant4 expects an exact distance to be returned, given the particle direction. In order to implement the *optimistic* method without modifying the `G4Navigator`, a static geometry must be mocked. In the following, we describe how this is done in `G4Turtle`.

A top level `Envelope` volume is defined. This volume is bounded by a top and bottom altitude, in ECEF coordinates. It contains two rock `Chunks` and two air `Chunks` sub volumes. These sub-volumes are artefacts used to steer the navigation. They have a variable position and extent. This requires disabling `SmartVoxels` navigation within the `Envelope`, since the algorithm doesn't support moving volumes. Geant4 starts by checking if a particle is inside the top volume, i.e. the envelope. At this stage we compute the particle altitude and the corresponding ground level using a `turtle_stepper`. If the particle is inside the `Envelope`, the Geant4 navigation will further check the sub-volumes. Given the particle altitude w.r.t. the ground, the rock or air chunks will return `kInside` or `kOutside`. Inside a `Chunk`, Geant4 requests the distance to the border. An *optimistic* estimate of the distance to the ground is returned, as given by pseudocode 3, i.e. refined with a binary search. When the navigation exits the chunk, it will start again checking if the particle is still inside the envelope. However, it won't check the chunk that was just exited. Therefore, two chunks of each material are needed.

The previous method needs to be slightly refined in order to handle extra volumes placed within the topography envelope, e.g. a detector. First, when Geant4 checks if the particle is inside the `Envelope` we loop over all extra sub-volumes, i.e. non `Chunks`. If the particle happens to be located in any of these sub-volumes, the rock and air chunks return `kOutside`, i.e. extra volumes have precedence over the topography. In addition, when computing the *optimistic* stepping distance from within a `Chunk`, we need to check the `DistanceToIn` to all extra sub-volumes. If any sub-volume is closer than the distance provided by eq. (1), the initial stepping distance is modified accordingly. If a binary search needs to be done, extra sub-volumes are checked again, at each iteration. Note that sub-volumes are traversed with a linear search since `SmartVoxels` navigation is disabled. Therefore, this implementation is not optimal if a large number of sub volumes is to be inserted inside the topography. `SmartVoxels` are however re-activated by default within sub-volumes, speeding up the navigation once inside one of them. So, complex sub volumes, e.g. a

detailed detector, should be manually enclosed in simple bounding `G4Box` when placed within the topography envelope.

The `G4Turtle` class was used with `Geantinos` in order to compute the rock depth for the three views described in section 4. For the optimal parameter values derived in section 5 an average agreement of $1\ \mu\text{m}$ was found with the direct computation using the TURTLE library. Discrepancies of a few mm could be observed for a few grazing rays. The Geant4 computation, using `G4Turtle` and `Geantinos` was 4 times slower than the direct one. In addition, the `G4Turtle` class was validated with μ using the `G4EmStandardphysics` and `G4EmExtraphysics` modular physics list. The corresponding test program is shipped with the sources of `G4Turtle`, as an example of usage. The performances depend strongly on the production cut value set when building the `physicsList`. Cut values below 1 m slow down the μ transport. The average CPU usage per Monte-Carlo step is rather constant though. The `G4Navigator` amounts to 15 % of the CPU instructions of a step. Half of these instructions are for calls to the TURTLE library. From these numbers it can be seen that though non optimal, the `G4Turtle` implementation already delivers excellent performances for stepping through topography data in Geant4. However, it does not allow to visualise the topography using one of the Geant4 3D rendering modes.

References

- [1] X-5 Monte Carlo Team. MCNP - Version 5, Vol. I: Overview and Theory. Technical Report LA-UR-03-1987, 2003. URL: https://laws.lanl.gov/vhosts/mcnp.lanl.gov/pdf_files/la-ur-03-1987.pdf.
- [2] D.B. Pelowitz et al. MCNPX 2.7.0 Extensions. Technical Report LA-UR-11-02295, 2011. URL: https://laws.lanl.gov/vhosts/mcnp.lanl.gov/pdf_files/la-ur-11-02295.pdf.
- [3] C. J. Werner et al. MCNP6.2 Release Notes. Technical Report LA-UR-18-20808, 2018. URL: https://laws.lanl.gov/vhosts/mcnp.lanl.gov/pdf_files/la-ur-18-20808.pdf.
- [4] S. Agostinelli et al. Geant4 - a simulation toolkit. *Nucl. Instrum. Methods Phys. Res. A*, 506(3):250 – 303, 2003. doi:10.1016/S0168-9002(03)01368-8.
- [5] J. Allison et al. Geant4 developments and applications. *IEEE Trans. Nucl. Sci.*, 53(1):270–278, Feb 2006. doi:10.1109/TNS.2006.869826.
- [6] J. Allison et al. Recent developments in Geant4. *Nucl. Instrum. Methods Phys. Res. A*, 835:186 – 225, 2016. ISSN 0168-9002. doi:10.1016/j.nima.2016.06.125.
- [7] G. Cosmo. The Geant4 geometry modeler. In *IEEE Symposium Conference Record Nuclear Science 2004*, volume 4, pages 2196–2198, Oct 2004. doi:10.1109/NSSMIC.2004.1462698.
- [8] C. M. Poole, I. Cornelius, J. V. Trapp, and C. M. Langton. Fast Tessellated Solid Navigation in Geant4. *IEEE Trans. Nucl. Sci.*, 59(4):1695–1701, Aug 2012. doi:10.1109/TNS.2012.2197415.

- [9] S. Mukherjee, P.K. Joshi, S. Mukherjee, A. Ghosh, R.D. Garg, and A. Mukhopadhyay. Evaluation of vertical accuracy of open source Digital Elevation Model (DEM). *Int. J. Appl. Earth Obs. Geoinf.*, 21:205 – 217, 2013. doi:10.1016/j.jag.2012.09.004.
- [10] A. M. Dziewonski and D. L. Anderson. Preliminary reference Earth model. *Phys. Earth Planet. In.*, 25(4):297 – 356, 1981. doi:10.1016/0031-9201(81)90046-7.
- [11] Valentin Niess. TURTLE : Topographic Utilities for tRansporting parTicules over Long rangEs, 2016–2018. URL: <https://niess.github.io/turtle/>.
- [12] Valentin Niess. The TURTLE Application Programming Interface, 2016–2018. URL: <https://niess.github.io/turtle-docs>.
- [13] NASA/METI/AIST/Japan Spacesystems and U.S./Japan ASTER Science Team. ASTER Global Digital Elevation Model [Data set]. NASA EOSDIS Land Processes DAAC, 2009. doi:10.5067/ASTER/ASTGTM.002.
- [14] NASA JPL. NASA Shuttle Radar Topography Mission Global 1 arc second [Data set]. NASA EOSDIS Land Processes DAAC, 2013. doi:10.5067/MEaSURES/SRTM/SRTMGL1.003.
- [15] Frank G. Lemoine et al. The NASA GSFC and NIMA Joint Geopotential Model. Technical Report NASA/TP-1998-206861, 1998. URL: <https://cddis.nasa.gov/926/egm96/TOC.HTML>.
- [16] D. K. Olson. Converting Earth-centered, Earth-fixed coordinates to geodetic coordinates. *IEEE Trans. Aerosp. Electron. Syst.*, 32(1):473–476, Jan 1996. doi:10.1109/7.481290.
- [17] V. Niess. PUMAS, Semi Analytical MUons -or taus- Propagation, backwards, 2016–2018. URL: <http://niess.github.io/pumas-pages>.
- [18] F. Ambrosino et al. Joint measurement of the atmospheric muon flux through the Puy de Dôme volcano with plastic scintillators and Resistive Plate Chambers detectors. *J. Geophys. Res. Solid Earth*, 120(11):7290–7307, 2015. doi:10.1002/2015JB011969.
- [19] Q. Zheng, X.-P. Wu, M. Johnston-Hollitt, J.-h. Gu, and H. Xu. Radio Sources in the NCP Region Observed with the 21 Centimeter Array. *Astrophys. J.*, 832:190, December 2016. arXiv:1602.06624, doi:10.3847/0004-637X/832/2/190.
- [20] D. Ardouin et al. First detection of extensive air showers by the TREND self-triggering radio experiment. *Astropart. Phys.*, 34:717–731, 2011. arXiv:1007.4359, doi:10.1016/j.astropartphys.2011.01.002.
- [21] Jaime Alvarez-Muñiz et al. The Giant Radio Array for Neutrino Detection (GRAND): Science and Design. 2018. arXiv:1810.09994.
- [22] J. R. Shewchuk. Triangle: Engineering a 2D Quality Mesh Generator and Delaunay Triangulator. In M. C. Lin and D. Manocha, editors, *Applied Computational Geometry: Towards Geometric Engineering*, volume 1148 of *Lecture Notes in Computer Science*, pages 203–222. Springer-Verlag, May 1996. From the First ACM Workshop on Applied Computational Geometry.
- [23] The CGAL Project. CGAL, Computational Geometry Algorithms Library, 2018. URL: <https://www.cgal.org>.

- [24] P. Alliez, S. Tayeb, and C. Wormser. 3D Fast Intersection and Distance Computation. In *CGAL User and Reference Manual*. CGAL Editorial Board, 4.13 edition, 2018. URL: https://doc.cgal.org/4.13/Manual/packages.html#PkgAABB_treeSummary.
- [25] N. Nethercote and J. Seward. Valgrind: A Framework for Heavyweight Dynamic Binary Instrumentation. In *Proceedings of the 28th ACM SIGPLAN Conference on Programming Language Design and Implementation*, pages 89–100. ACM, 2007. doi:10.1145/1250734.1250746.
- [26] J. Weidendorfer, M. Kowarschik, and C. Trinitis. A Tool Suite for Simulation Based Analysis of Memory Access Behavior. In *Computational Science - ICCS 2004*, pages 440–447. Springer Berlin Heidelberg, 2004. doi:10.1007/978-3-540-24688-6_58.
- [27] V. Niess, A. Barnoud, C. Cârloganu, and E. Le Ménédeu. Backward Monte-Carlo applied to muon transport. *Comput. Phys. Commun.*, 229:54–67, 2018. arXiv:1705.05636, doi:10.1016/j.cpc.2018.04.001.
- [28] Igor A. Sokalski, Edgar V. Bugaev, and Sergey I. Klimushin. MUM: Flexible precise Monte Carlo algorithm for muon propagation through thick layers of matter. *Phys. Rev. D*, 64:074015, Sep 2001. doi:10.1103/PhysRevD.64.074015.
- [29] Valentin Niess. G4TURTLE : Geant4 Topographic Utilities for tRansporting parTicules over Long rangEs, 2018. URL: <https://niess.github.io/turtle-geant4/>.